Journal of Hazardous Materials Advances 23 (2026) 101457

Contents lists available at ScienceDirect

Journal of Hazardous Materials Advances

journal homepage: www.elsevier.com/locate/hazadv

Random Forest-based spatial distribution from heavy metals and associated with ecological and health risk assessment in agricultural soils of the Mantaro Valley, Peru

Edith Orellana-Mendoza [a,*], Roberto Cosme [b], Violeta Quispe-Coquil [c], Katia Mendoza [d], Sheila Valero-Maraví [a], Ángeles Rojas-León [a], Dennis Ccopi [e], Samuel Pizarro [e,f]

[a] Facultad de Ingeniería Forestal y Ambiental, Universidad Nacional del Centro del Perú, Av. Mariscal Castilla 3909-4089, Huancayo, 12006, Peru
[b] Instituto Nacional de Innovación Agraria (INIA), Av. La Molina 1981, Lima, 15024, Peru
[c] Facultad de Ingeniería Química, Universidad Nacional del Centro del Perú, Huancayo, Peru
[d] Estación Experimental Agraria Canaán, Av. Abancay 299, Huamanga, Ayacucho, Peru
[e] Dirección de Servicios Estratégicos Agrarios, Instituto Nacional de Innovación Agraria (INIA), Carretera Saños Grande - Hualahoyo Km 8 Santa Ana, Huancayo, Junín, 12006, Peru
[f] Instituto de Investigación para el Desarrollo Sustentable de Ceja de Selva (INDES-CES), Universidad Nacional Toribio Rodríguez de Mendoza de Amazonas, Chachapoyas, 01001, Peru

A R T I C L E I N F O

Keywords:
Random Forest
Soil contamination
Ecological risk indices
Non-carcinogenic risk
Carcinogenic risk
Machine learning
Heavy metals

A B S T R A C T

Heavy metal (HM) contamination of agricultural soils in Andean valleys poses a critical threat to ecological integrity, food safety, and human health. This study assessed the spatial distribution, contamination levels, ecological and health risk (non-carcinogenic and carcinogenic) associated with Zn, Pb, Cu, Cd, and As in agricultural soils of the Mantaro Valley in the central Andes of Peru. A total of 306 topsoil samples were analyzed. Random Forest (RF) was used to model the spatial distribution of HM concentrations, integrating spectral, climatic, topographic, edaphic, and distance-related covariates. The RF models showed consistent but element-specific predictive performance. The values of R^2 ranged from 0.76 to 0.89, with the highest values for Pb and As and the lowest for Cu. Spatial predictions should be interpreted with consideration of the irregular sampling design and inherent uncertainties in spatial extrapolation. Mean concentrations of Zn, Pb, Cu, As, and Cd reached 1347.87, 439.91, 201.71, 90.69, and 4.27 mg kg^{-1}, respectively, exceeding both regulatory thresholds and local geochemical background values. Contamination indices revealed marked enrichment, particularly for As and Cd. Ecological risk was primarily driven by Cd and As, with 70.10% and 61.41% of samples classified as very high ecological risk for these elements, respectively. The comprehensive potential ecological risk index indicated a critical scenario with 71.7% of samples exceeding the very high-risk threshold. Human health risk assessment identified As as the main contributor to both non-carcinogenic and carcinogenic risks, with children showing higher vulnerability than adults. These findings delineate priority agricultural areas where ecological risk and arsenic-related carcinogenic risk overlap, underscoring the urgent need for targeted soil monitoring, exposure reduction, and locally adapted risk management strategies in the Mantaro Valley.

1. Introduction

Agricultural soils can act as long-term sinks for HM derived from both geogenic processes and anthropogenic activities, including mining, smelting, wastewater irrigation, atmospheric deposition, vehicular traffic, and the intensive use of fertilizers and pesticides (Huang et al., 2019; Keshavarzi et al., 2021). Once introduced into the soil, HM may persist for extended periods, interact with mineral and organic fractions, and become available for plant uptake or human exposure through ingestion, inhalation, and dermal contact (Gao et al., 2021). Among the most environmentally relevant HM, As, Cd, Pb, and Hg are of particular concern due to their high toxicity and the adverse effects associated with chronic exposure, including neurological disorders, kidney damage, and carcinogenic outcomes (Huang et al., 2017; Järup, 2003; Mushak, 2011;

* Corresponding author.
E-mail addresses: eporellana@uncp.edu.pe (E. Orellana-Mendoza), samuel.pizarro@untrm.edu.pe (S. Pizarro).

https://doi.org/10.1016/j.hazadv.2026.101457
Received 2 March 2026; Received in revised form 9 July 2026; Accepted 30 July 2026
Available online 31 July 2026

Zhao et al., 2019). These elements may pose significant risks even at relatively low concentrations, depending on their chemical speciation, bioavailability, exposure pathway, and duration of exposure. In contrast, essential trace elements such as Cu, Zn, and Ni play important physiological roles in living organisms; however, excessive concentrations can disrupt cellular functions and impair the quality and sustainability of agricultural ecosystems (Sanad et al., 2025). Consequently, the accumulation of HM in agricultural soils may adversely affect soil quality, crop productivity, food safety, and human health, particularly in intensively cultivated regions exposed to multiple contamination sources (Jiang et al., 2020; Nagajyoti et al., 2010; Nematollahi et al., 2020).

The assessment of HM contamination in agricultural soils has been widely conducted using geochemical and ecological indices, including the contamination factor (Cf), enrichment factor (EF), geoaccumulation index (Igeo), and potential ecological risk index (RI) (Chen et al., 2023a; Liu and Wang, 2024; Mitran et al., 2024; Oguntuase et al., 2024). These approaches provide valuable tools for evaluating the degree of HM accumulation in soils and their potential ecological implications. However, many studies remain focused on point-based concentration assessments, with limited consideration of the spatial heterogeneity of contaminants and the associated human exposure within complex agricultural systems (Zhang et al., 2023). Furthermore, although numerous studies have documented ecological and human health risks associated with HM exposure through ingestion, inhalation, and dermal contact pathways (Wang et al., 2025a; Wang et al., 2025c; Zhang et al., 2019), integrated assessments remain scarce for Andean agroecosystems historically affected by mining and metallurgical activities. Such assessments are particularly relevant in regions where long-term contamination, intensive agricultural production, and human exposure may coexist, potentially increasing environmental and public health concerns.

Analyzing the spatial distribution of HM contamination, ecological risk, and human health risk remains challenging because metal concentrations in agricultural soils are controlled by non-linear interactions among parent material, topography, hydrological connectivity, land use, soil properties, and anthropogenic inputs (Taghizadeh-Mehrjardi et al., 2021). Conventional geostatistical methods, such as ordinary kriging and regression kriging, have been widely used for soil contaminant mapping; however, their performance may be limited when relationships between metal concentrations and environmental covariates are complex or spatially non-stationary (Hengl et al., 2018; Qu et al., 2024b; Yang et al., 2021). More recently, machine-learning approaches, including XGBoost and hybrid models, have been increasingly applied to improve spatial predictions (Ye et al., 2023; Yu et al., 2025). Among these methods, Random Forest (RF) has gained considerable attention due to its ability to capture complex non-linear relationships and generate robust predictions from heterogeneous environmental datasets.

In this context, the integration of field-sampled HM data with multisource environmental covariates within a RF framework enables spatially explicit predictions of contamination levels, ecological risk, and carcinogenic risk, moving beyond conventional point-based assessments and providing spatially continuous risk information directly applicable to environmental monitoring and management in mining-influenced Andean agroecosystems (Lemenkova, 2024; Li et al., 2025a). RF originally developed by Breiman (2001), is particularly suitable because it can model non-linear relationships, handle high-dimensional predictor sets, reduce sensitivity to overfitting through ensemble learning, and estimate the relative importance of environmental covariates (Hengl et al., 2018; Louppe, 2014). Previous studies have successfully applied RF to predict the spatial distribution of HM in agricultural and urban soils using multisource environmental covariates, including remote sensing, topographic, climatic, and soil-property variables (Shi et al., 2021; Wang et al., 2020b; Xu et al., 2024). Nevertheless, a major challenge remains in selecting meaningful predictor variables and translating spatial predictions into contamination, ecological-risk, and health-risk maps that are useful for environmental management, particularly in Andean agricultural valleys affected by long-term mining and metallurgical activity.

In Peru, only 6% of the national territory is suitable for agricultural use, which significantly limits the availability of productive soils compared to other South American countries (Díaz, 2016). Among these areas, the Mantaro Valley, located in the Junín region, represents one of the most important agricultural systems in the central Andean region, supplying Lima and other parts of the country with key food crops such as maize, potato, artichoke, fava bean, and carrot. However, this agroecosystem has been exposed for more than eight decades to the influence of mining and metallurgical activities in the upper Mantaro River basin, particularly those associated with the La Oroya metallurgical complex (Loayza Muro, 2016). These activities have included the processing, smelting, and refining of polymetallic ores, with historical atmospheric emissions, contaminated sediments, and waste discharges containing elements such as Pb, Zn, Cu, Cd, and As. In addition, the Mantaro River has historically received untreated mining effluents, and its continuous use as an irrigation source may have contributed to the progressive accumulation of HM in agricultural soils of the valley (Custodio et al., 2020; MINAGRI, 2011). This chronic exposure to multiple contamination pathways may pose risks to soil quality, food safety, and public health, particularly within an intensive agricultural production system oriented toward local and national consumption. This chronic exposure to multiple contamination pathways may pose risks to soil quality, food safety, and public health, particularly within an intensive agricultural production system oriented toward local and national consumption. This concern is supported by regional evidence documenting Pb, As, and Cd contamination and child health impacts in La Oroya, as well as human health risks associated with exposure to HM and As in mining-influenced river waters of the central Peruvian Andes (Custodio et al., 2019, 2021; Reuer et al., 2012).

Previous studies have reported elevated levels of As, Pb, Cu, Fe, and Zn in agricultural soils at specific locations within the Mantaro Valley (Custodio et al., 2020; Orellana et al., 2019). However, a critical gap remains in understanding the spatial patterns of HM accumulation and the factors controlling their distribution in the valley's soils. In this context, the application of machine learning algorithms, such as RF represents an innovative and robust approach for modeling complex non-linear relationships among edaphic variables, environmental factors, and metal concentrations. The generation of high-resolution spatial maps based on RF will enable more accurate estimation of contamination levels, potential ecological risk, and human health risk in a high-Andean agroecosystem exposed to more than eight decades of mining and metallurgical activities. Therefore, the identification of critical accumulation hotspots may contribute to the development of targeted contaminant monitoring strategies and the implementation of sustainable agricultural management practices.

Based on the long-term influence of mining and metallurgical activities in the upper Mantaro River basin, the intensive agricultural use of the valley, and the potential role of environmental covariates in controlling HM accumulation, we hypothesized that HM concentrations and associated risks are spatially heterogeneous and mainly influenced by soil properties, hydrological connectivity, proximity to roads and rivers, and historical contamination pathways. Therefore, this study aimed to: (1) assess the concentrations and spatial distribution of As, Cd, Pb, Cu, and Zn in agricultural soils of the Mantaro Valley using the Random Forest (RF) model; (2) estimate contamination levels, potential ecological risk, and human health risk associated with these HM; and (3) identify critical contamination and risk hotspots to provide baseline information for environmental monitoring, mitigation strategies, and sustainable soil management in this intensively cultivated Andean valley.

2. Materials and methods

2.1. Study area

The study was carried out in the irrigated and non-irrigated agricultural areas of the Mantaro Valley, which includes the provinces of Huancayo, Concepción, Jauja, and Chupaca, located in the department of Junín. The study area lies between latitudes 12.2377°S and 11.6793°S, and longitudes 75.5792°W and 75.1202°W, covering a total area of 635.22 km^2 (Fig. 1), with elevations ranging from 3150 to 3370 m above sea level.

The Mantaro Valley is located in the central Andes of Peru and is shaped by the Mantaro River, which flows through the alluvial plain from north to south, dividing the valley into two margins. The main economic activities in the region are agriculture and commerce (Álvarez-Tolentino and Suárez-Salas, 2020).

The Mantaro Valley has a mean annual temperature of 11.9°C, with minimum temperatures ranging from 4.0 to 5.5°C and maximum temperatures varying between 16.5 and 21.5°C (Sandoval et al., 2022). Precipitation is characterized by two well-defined seasons: a dry season extending from June to September and a wet season from October to May, with the highest rainfall occurring in January and February. The average annual precipitation is approximately 750 mm (Álvarez-Tolentino and Suárez-Salas, 2020). The valley soils are predominantly characterized by medium-textured classes (sandy loam, loam, and sandy clay loam), slightly alkaline pH values (7.2–8.0), and a moderate mean soil organic matter content of 3.72%. The valley is surrounded by mountain ranges and traversed by the Mantaro River. The left bank is broader and relatively flat, containing most of the river tributaries and representing the most urbanized sector of the valley. In contrast, the right bank is narrower and steeper, where small-scale agricultural and livestock-production districts are predominantly located.

2.2. Sample collection, preparation and analysis

A total of 306 representative composite surface soil samples were collected from a 0–20 cm depth across agricultural areas within the Mantaro Valley study region, corresponding to the main arable layer directly influenced by tillage, irrigation, fertilizer application, pesticide use, and soil–crop interactions. Sampling locations were selected using a Latin Hypercube Sampling strategy to capture the environmental variability of the agricultural landscape, considering gradients related to climatic conditions, topography, soil properties, spectral characteristics, and proximity to rivers and roads. This approach is suitable for digital soil mapping because it allows sampling points to be distributed across the environmental covariate space rather than following a strictly regular grid, thereby improving the representation of soil variability across heterogeneous agricultural landscapes (Carbajal-Llosa et al., 2025; Pizarro et al., 2023). Each composite sample was obtained within a single agricultural plot by combining and homogenizing 5 to 7 subsamples, which were randomly collected along a diagonal transect with inter-subsample distances ranging from 25 to 50 m, following national soil sampling protocols (MINAM, 2014). Thus, each sampling location

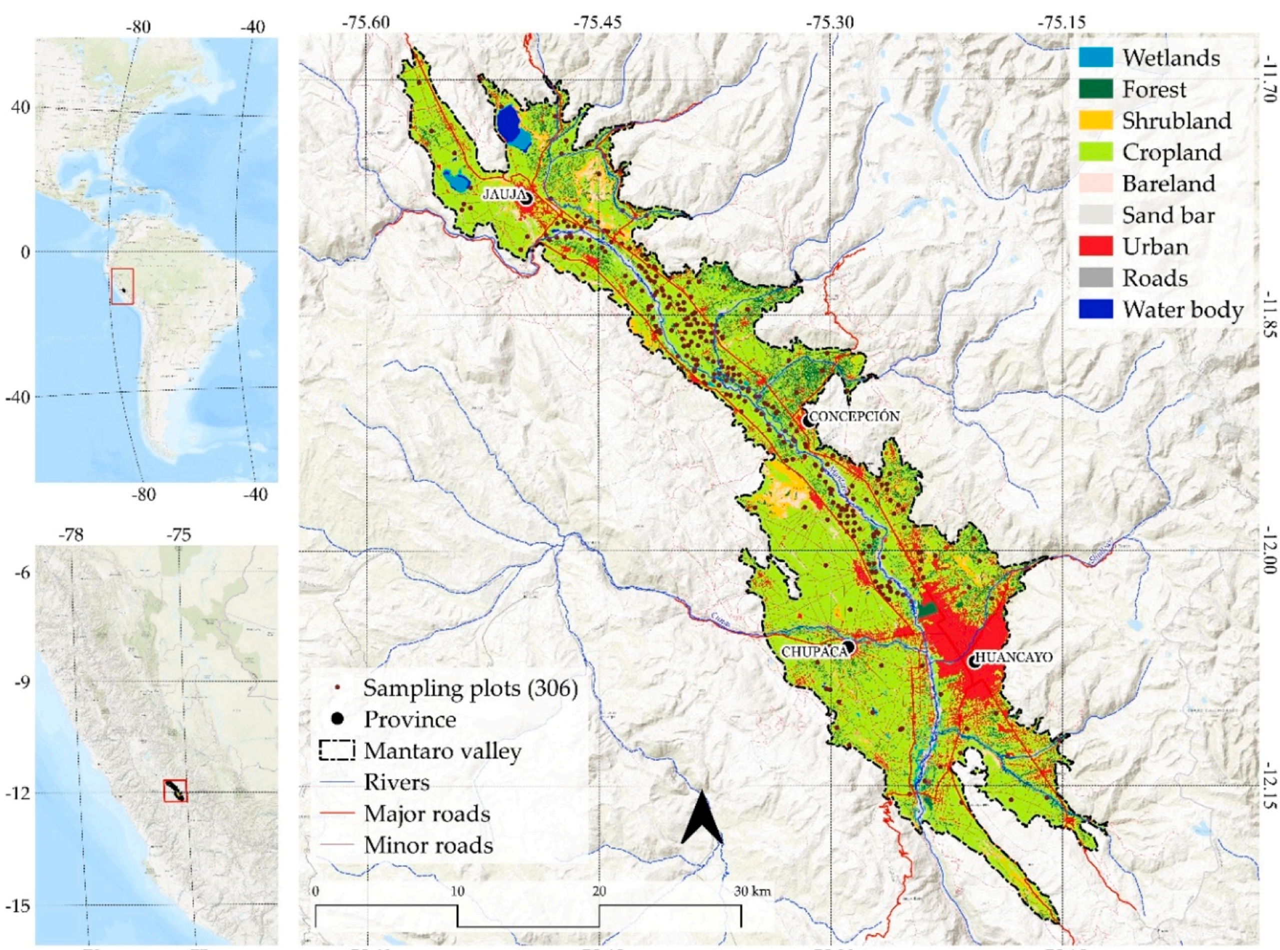

Fig. 1. Geographical location of the study area and distribution of the 306 soil sampling sites in the Mantaro Valley, Junín Region, central Peru. Sampling locations are distributed across agricultural lands within four provinces of the valley.

generated one representative composite sample of the plot. Geographic coordinates of each sampling point were recorded using a Global Positioning System (GPS) device, with inter-site distances ranging from 1 to 3 km.

Following field collection, composite samples (approximately 1.0 kg each) were transported to the laboratory in airtight polyethylene bags under proper chain-of-custody procedures. Laboratory processing involved drying the samples under controlled laboratory conditions at room temperature (20 ± 2°C) for 10 days until constant mass was achieved. Physical contaminants, including plant residues, stones, and organic debris, were manually removed to ensure sample homogeneity. The dried samples were subsequently ground using a mortar and pestle and sieved through a 2 mm stainless steel mesh to obtain the <2 mm fine earth fraction suitable for chemical analysis. A 100 g aliquot was taken from each preprocessed sample for the determination of HM concentrations, specifically As, Cd, Pb, Cu, and Zn. Prepared samples were stored in airtight polyethylene bags under controlled laboratory conditions and analyzed within 30 days to minimize potential contamination.

2.3. Soil samples digestion, analysis, and quality control

HM concentrations were determined through microwave-assisted acid digestion followed by inductively coupled plasma mass spectrometry (ICP-MS) analysis. A 0.5 g aliquot of each prepared soil sample was subjected to acid digestion using 9.0 mL of ultrapure nitric acid (HNO_3) and 3.0 mL of ultrapure hydrochloric acid (HCl) in a microwave-assisted digestion system, following the standardized EPA 3051A protocol (USEPA, 2007). The resulting digestates were analyzed for As, Cd, Pb, Cu y Zn concentrations using a Perkin Elmer NexION 2000X ICP-MS instrument. Comprehensive quality assurance procedures were implemented to ensure analytical accuracy and precision. Each analytical batch included reagent blanks, duplicate samples, continuing calibration verification (CCV) standards, and certified reference materials (CRM). CCV recoveries ranged from 94.8% to 102.0%, and CRM recoveries ranged from 101.7% to 108.95% indicating acceptable analytical accuracy for As, Cd, Pb, Cu, and Zn. Relative standard deviations remained below 5%, reflecting adequate analytical precision and reproducibility. The detection limits (mg kg^{-1}) were 0.03, 0.02, 0.07, 0.07 and 0.14 for As, Cd, Pb, Cu, and Zn, respectively. Detailed analytical quality-control parameters including CCV recovery, and certified reference material recovery for all analyzed elements, are provided in Table S1.

2.4. Predictive spatial analysis of HM contamination

RF regression was employed to generate spatial distribution maps of As, Cd, Cu, Pb, and Zn concentrations. RF was selected as a widely used machine-learning algorithm capable of modeling complex relationships between heavy metal concentrations and environmental covariates, including soil properties, climatic variables, topographic attributes, and proximity to rivers and roads (Grimm et al., 2008). Separate RF models were developed for each element using the complete dataset of 306 soil samples. Individual RF models were developed for each element using the complete dataset of 306 soil samples, with hyperparameters including mtry (5–23), number of trees (50–500), and bag fraction (0.1–0.9) optimized through a systematic grid search using 5-fold cross-validation for each element-specific model. Model performance was evaluated based on the coefficient of determination (R^2), root mean square error (RMSE), mean squared error (MSE), and mean absolute error (MAE), derived from cross-validation. In this study, RF was applied as a predictive tool to generate spatially explicit HM concentration layers, which were subsequently used as inputs for the calculation of contamination indices, ecological risk, non-carcinogenic risk, and carcinogenic risk across the agricultural landscape. It should be noted that the 10 m spatial resolution of the generated prediction maps reflects the native resolution of the environmental covariates, particularly Sentinel-2-derived spectral layers, rather than the effective prediction resolution supported by the sampling density. Given the inter-site spacing of 1–3 km, the spatial outputs should be interpreted as screening-level products for identifying priority contamination and risk areas, rather than as site-specific predictions at fine spatial scales.

The predictor variable framework encompassed five primary categories: climate variables, topographic attributes, spectral indices, soil physicochemical properties, and spatial distance metrics (Fig. S1), following the comprehensive approach proposed by Pizarro et al. (2025a). Covariates were selected following a two-step procedure. First, variables were included based on their known influence on HM retention, mobility, and accumulation in soils, encompassing climatic, topographic, spectral, edaphic, and distance-related predictors. Second, a decorrelation analysis was applied using a Pearson correlation threshold of r = 0.80 to remove redundant predictors and minimize multicollinearity before model fitting (Table 1). All covariate layers were standardized to 10 m spatial resolution and processed within the Google Earth Engine (GEE) cloud computing platform.

2.4.1. Model selection and performance evaluation

The optimal predictive model for each element was selected through the evaluation of three performance metrics calculated from k-fold cross-validation: R^2, RMSE, and MAE (Qu et al., 2024a; Zhang et al., 2020). The coefficient of determination quantifies the proportion of variance in the dependent variable explained by the independent variables, with values approaching unity indicating superior model performance and closer approximation to the 1:1 line (Qu et al., 2024a). The RMSE metric quantifies the standard deviation of prediction residuals, representing the magnitude of differences between predicted and observed values, while MAE provides the average absolute prediction error (Xu et al., 2024). Models exhibiting lower RMSE and MAE values demonstrate enhanced prediction accuracy and reduced systematic error.

2.4.2. Variable importance analysis

To improve model interpretability and evaluate the contribution of each predictor variable to HM spatial prediction, variable importance analysis was conducted for each element-specific RF model (Nguyen et al., 2020). This analysis quantified the relative contribution of each

Table 1
Spatial covariables included in the spatial modeling.

Category	Variables	Rationale
Spectral indices	NDVI (normalized difference vegetation index); NDWI (normalized difference water index); SAVI (soil-adjusted vegetation index); EVI (enhanced vegetation index); RI (redness index). (Sentinel-2)	Indirectly reflect vegetation vigor and soil surface conditions, which may influence metal uptake and erosion (Pizarro et al., 2023).
Topography	Elevation, slope, aspect, eastness, northness, Gaussian curvature, horizontal/vertical/mean curvature.	Influence runoff, deposition, and accumulation zones of contaminants (Zhuang et al., 2021) .
Climatic	PET (Reference evapotranspiration), Tmax (maximum temperature); Tmin (minimum temperature); precipitation. (WorldClim v2.1)	Control soil moisture and weathering rates, affecting metal mobility (Shaikh et al., 2021).
Soil properties	Clay, sand, silt, pH, CEC (cation exchange capacity); BDOD (bulk density of the fine earth fraction), SOC (soil organic carbon content); nitrogen (total nitrogen). (Soil Grids v2.0)	Affect metal retention, solubility, and bioavailability (Alloway, 2013) .
Distance metrics	Distance to rivers (D_Riv); distance to major and minor roads ((D_mjR and D_mnR) .	Indicate potential contamination sources (e.g., mining, transport) (Liu et al., 2003) .

environmental covariate to predictive performance, allowing the identification of the dominant climatic, topographic, spectral, edaphic, and distance-related factors associated with the spatial distribution of each element. Therefore, variable importance was used as an RF-based interpretability approach to support the environmental interpretation of HM distribution patterns (Ishwaran and Kogalur, 2010).

2.4.3. Spatial prediction and uncertainty quantification

Following model selection, the optimal RF models were applied to georeferenced raster layers containing the selected predictor variables to generate spatially explicit predictions of As, Cd, Cu, Pb, and Zn concentrations at the pixel scale. Prediction uncertainty was quantified by iteratively applying the k-fold RF models to the predictor stack, generating multiple predictions for each pixel. The variance among these predictions was calculated and expressed as percentage values to represent relative spatial prediction uncertainty (Kim et al., 2018). Model performance and uncertainty were further evaluated using cross-validation metrics (R^2 and RMSE) and residual analysis, which was used to identify systematic prediction errors and potential biases across the concentration range of each element (Fig. S2). The resulting concentration and uncertainty maps were subsequently used to support contamination assessment, ecological risk evaluation, and human health risk assessment, while also identifying areas where model predictions may be less reliable. Risk calculations were performed using raster-based operations in the R statistical environment (R Core Team, 2023), through the terra package, enabling pixel-by-pixel computation of contamination indices and risk metrics across the entire study domain.

2.5. Contamination and potential ecological risk index assessment

2.5.1. Contamination factor (Cf)

Cf is an indicator of contamination by anthropogenic inputs associated with a single HM (Hakanson, 1980), it quantifies the ratio between the concentration of each metal in the soil (C_m) and the concentration in the uncontaminated soil ($C_{background}$, geochemical background value). The geochemical background values were (mg/kg): As = 1.5, Cd =0.098, Cu = 25, Pb = 20 and Zn = 71 (Taylor and McLennan, 1995). Hakanson classifies Cf into four categories: Low (CF < 1), moderate (1 ≤ CF < 3), considerable (3 ≤ CF < 6), and very polluted (CF ≥ 6) (Sharafi and Salehi, 2025). It is calculated according to the Eq. (1):

$$C_f = \frac{C_m}{C_{background}} \tag{1}$$

2.5.2. Index of geoaccumulation (Igeo)

The index of geoaccumulation is used to assess the level of pollution with metals in soil and sediments caused by natural or anthropogenic sources (Gong et al., 2022; Muller, 1969; Vasudhevan et al., 2025). Igeo is measured by Eq. (2).

$$Igeo = log2\frac{C_m}{1.5 \times C_{background}} \tag{2}$$

Where C_m shows measured metal contents in samples, $C_{background}$ symbolize reference or background values of metal, 1.5 is a factor that is used to calculate possible changes in background value. The standard for classifying the geoaccumulation index is as follows: Uncontaminated (Igeo ≤ 0), uncontaminated to moderately (0 ≤ Igeo < 1), moderately (1 ≤ Igeo < 2), moderately to heavily (2 ≤ Igeo < 3), heavily (3 ≤ Igeo < 4), heavily to extremely (4 ≤ Igeo < 5), and extremely contaminated (Igeo ≥ 5).

2.5.3. Potential ecological risk index

The potential ecological risk index (RI) is calculated based on the concentration of HM, their toxic response factors, and their contamination levels in soil (Wu et al., 2021). This method was proposed by Hakanson (1980) and Kang et al. (2020) to assess the potential impact of HM on ecosystems (soil and sediments), using the Eqs. (3) and (4):

$$RI = \sum_{i=1}^{n} T_r^i \, C_f \tag{3}$$

$$ER = T_r^i \, C_f \tag{4}$$

where *RI* is the total potential ecological risk index, *ER* is the individual ecological risk of each element, T_r^i is the toxic response factor for each metal (Cd = 30, As = 10, Pb = 5, Cu= 5 and Zn = 1) (Zerizghi et al., 2022). In order to more accurately reflect the current states of contamination, the levels of *ER* and *RI* were adjusted to improve the precision of ecological risk classification, as proposed by Cai et al. (2024) and Li et al. (2025b). The ecological risk (*ER*) for each metal was classified into five categories: Low (*ER*<30), moderate (30≤*ER*<60), considerable (60≤*ER*<120), high (120≤*ER*<240), and very high risk (*ER*≥240). Similarly, the comprehensive potential ecological risk index (*RI*) was classified into five risk classes: Low (*RI*<60), moderate (60 ≤ *RI*<120), considerable (120≤ *RI*< 240), high (240≤ *RI*< 480), and very high risk (*RI* > 480).

2.6. Health risk assessment

The human health risks associated with toxic metals in soil were assessed using the human health risk assessment methodology proposed by the United States Environmental Protection Agency (USEPA, 2001, 2019). Both non-carcinogenic and carcinogenic risks were evaluated for adults and children through three exposure pathways: oral ingestion, dermal contact, and inhalation (Gan et al., 2022). The assessment of the three exposure pathways was calculated according to the following Eqs. (5)–(7) (Ahmad et al., 2025; Li et al., 2024, 2024):

$$ADI_{ing} = \frac{C_{soil} \times IR_{soil} \times EF \times ED}{BW \times AT} \times 10^{-6} \tag{5}$$

$$ADI_{der} = \frac{C_{soil} \times SA \times AF \times ABS \times EF \times ED}{BW \times AT} \times 10^{-6} \tag{6}$$

$$ADI_{inh} = \frac{C_{soil} \times IR_{inh} \times EF \ x \ ED}{PEF \times BW \times AT} \tag{7}$$

where ADI*ing*, ADI*der* y ADI*inh* represent the average daily intake (mg/kg/day) of HM in soil through ingestion, dermal contact, and inhalation, respectively. C*soil* is the mean concentration of the heavy metal in soil samples (mg/kg). IR*soil* denotes the soil ingestion rate (50 mg/day for adults and 200 mg day⁻1 for children); IR*inh* is the inhalation rate (15 m^3 day⁻1 for adults and 10 m^3 day⁻1 for children); EF is the exposure frequency (180 days $year^{-1}$ for adults and 250 days $year^{-1}$ for children); ED is the exposure duration (25 years for adults and 6 years for children); BW is the average body weight of the exposed individual (70 kg for adults and 15 kg for children); AT is the averaging time (9125 days for adults and 2190 days for children); PEF is the particle emission factor (5.0E−06 m^3 kg^{-1} for adults and 8.0E−06 m^3 kg^{-1} for children); SA is the exposed skin surface area (4500 cm^2 for adults and 2500 cm^2 for children); AF is the dermal adherence factor (0.002 mg cm^{-2} for adults and 0.003 mg cm^{-2} for children); and ABS is the dermal absorption factor (0.001 for adults and 0.003 for children) (Pizarro et al., 2025b).

Based on the ADI values, the hazard quotient (HQ) and hazard index (HI), which represent the non-carcinogenic health effects of individual HM and the combined effects of all HM, respectively, were calculated using Eqs. (8) and (9):

$$HQ = \frac{ADI_{ing}}{RfD_{ing}} + \frac{ADI_{der}}{RfD_{der}} + \frac{ADI_{inh}}{RfD_{inh}} \tag{8}$$

$$HI = \sum_{i=1}^{n} HQ_{(i)} \tag{9}$$

where RfD (mg kg^{-1} day^{-1}) is the reference dose. If the HQ and HI values are < 1, the non-carcinogenic exposure risk is considered negligible or insignificant; if these values exceed 1, a significant non-carcinogenic risk is assumed. Conversely, the carcinogenic risk (CR) and total carcinogenic risk (TCR) posed by individual toxic metals and by the combined effects of all toxic metals were calculated using Eqs. (10) and (11):

$$CR = ADI_{ing} \times SF_{ing} + ADI_{der} \times SF_{der} + ADI_{inh} \times SF_{inh} \tag{10}$$

$$TCR = \sum_{i=1}^{n} CR_{(i)} \tag{11}$$

where SF (mg kg^{-1} day^{-1}) is the lifetime cancer slope factor. Carcinogenic risk is considered negligible when CR and TCR are below 10^{-6}, acceptable or tolerable between 10^{-6} and 10^{-4}, and high when exceeding 10^{-4}, indicating significant and unacceptable health risks (Auritro et al., 2026; Wang et al., 2025b).

3. Results and discussion

3.1. Descriptive statistical analysis of HM contents in soil

The concentrations of HMs in the agricultural soils of the Mantaro Valley are presented in Table 2. Mean concentrations (mg kg^{-1}) followed the decreasing order Zn (1347.87) > Pb (439.91) > Cu (201.71) > As (90.69) > Cd (4.27). Zn, Pb y Cu showed the highest concentrations, while As y Cd showed relatively lower concentrations, but they remain environmentally relevant due to their toxicity and persistence. The average concentrations of As, Cd, Pb, Cu, and Zn exceeded the maximum permissible limits established by national regulations (MINAM, 2017), as well as geochemical background values, by approximately 18.9, 21.9, 8.1, 60.5, and 43.6 times, respectively, reflecting significant accumulation of these elements within the agricultural ecosystem. The wide concentration ranges and the differences between mean and median values indicate asymmetric distributions, particularly for Zn and Pb. The maximum concentrations of Zn (10,051.27 mg kg^{-1}) and Pb (5674.35 mg kg^{-1}) were much higher than their respective median values, suggesting that the highest concentrations are concentrated in specific sectors rather than being evenly distributed across the valley. This pattern is consistent with localized enrichment processes superimposed on a broader pattern of diffuse contamination.

The coefficients of variation (CV) for HM ranged from 44% to 102%, following the order Cu > Pb > As > Zn > Cd. The high CV of Cu, Pb, As y Zn indicate strong dispersion and spatial heterogeneity, suggesting that their accumulation is controlled by uneven inputs and local soil conditions rather than by a single uniform source. From a geochemical perspective, this variability may reflect differences in element mobility, retention by soil components, and the spatial influence of mining-derived materials, atmospheric deposition, irrigation inputs, and agricultural practices (Liu et al., 2023; Rezapour et al., 2022; Tang et al., 2019). In contrast, Cd showed the lowest CV, suggesting a comparatively more homogeneous distribution across the sampled soils, although its mean concentration still exceeded the EQSS value (Li et al., 2023). Therefore, the CV values provide complementary evidence that HM contamination in the Mantaro Valley results from both localized hotspots and diffuse enrichment processes, with each element showing a distinct spatial behavior according to its sources and geochemical properties (Chen et al., 2023a).

Therefore, the variability of HM concentrations observed across the study area, as reflected by their coefficients of variation, may be largely controlled by soil properties that influence metal mobility and retention, including pH, redox potential, texture, organic matter content, and clay mineralogy (Rammal et al., 2025; Udeigwe et al., 2011). In particular, under slightly alkaline conditions (pH 7.2–8.0), the mobility of most metal cations tends to decrease due to adsorption and precipitation processes (Sharafi et al., 2026). Future studies should evaluate soil profiles to better understand the vertical mobility and leaching of HMs in Andean agricultural soils.

3.2. Principal component analysis PCA

The PCA shown in Fig. 2 explained 26.0% of the total variability through Dim1 (15.8%) and Dim2 (10.2%), reflecting the complexity of the agricultural landscape where HM distribution is controlled by multiple interacting factors. Given this limited explained variance, the PCA should be interpreted as an exploratory analysis of general association trends rather than a definitive characterization of HM-covariate relationships. Zn, Cu, and As were more closely related to soil physicochemical variables such as bulk density (BDOD), clay and silt contents, and pH, suggesting a possible influence of edaphic properties on their distribution. Similarly, soil organic carbon (SOC) and cation exchange capacity (CEC) were mainly associated with As and Zn, which is consistent with their potential role in metal retention within the soil matrix. In contrast, Cd and Pb showed a stronger relationship with sand content, precipitation, and some topographic variables, which could reflect a greater influence of environmental conditions and surface or hydrological transport processes. These preliminary trends complement the RF-based variable importance analysis and spatial interpretation of HM contamination in the agricultural soils of the valley, and should not be interpreted as definitive evidence of causal relationships.

These trends are consistent with known differences in the geochemical behavior of the evaluated elements. Zn is commonly associated with secondary minerals and stable oxides, which can reduce its mobility and favor relationships with soil properties such as pH, clay content, and cation exchange capacity (Wei et al., 2023). By contrast, Cd can be linked to more labile phases, including carbonate minerals, which increases its mobility under variable environmental conditions (Wei et al., 2023; Zhang et al., 2023). This higher sensitivity may also be influenced by moisture, hydrological dynamics, and local climatic conditions (González-Alcaraz et al., 2018). In addition, seasonal factors and sediment characteristics can modify the distribution of Cd and Zn in contaminated environments (Ruelas-Inzunza et al., 2009). Taken together, these findings suggest that the concentration and distribution of As, Cd, Cu, Pb and Zn in the agricultural soils of the Mantaro Valley may be governed by edaphic, climatic, topographic and spatial variables. Therefore, the associations identified in the PCA are presented as

Table 2
Statistical values of HM content in soil (mg/kg).

HM	Min	Max	Range	Median	Mean	SD	CV	EQSS
Zn	127.56	10,051.27	9923.71	1079.90	1347.87	973.87	0.72	200
Cd	0.58	22.45	21.88	4.27	4.27	1.87	0.44	1.4
Pb	26.79	5674.35	5647.56	258.41	439.91	436.49	0.99	70
As	22.42	705.96	683.54	66.97	90.69	68.13	0.75	50
Cu	20.49	1335.23	1314.75	98.88	201.71	206.06	1.02	ND

Min, minimum value; Max, maximum value; SD, standard deviation; CV, coefficient of variation; EQSS, environmental quality standard for soil (MINAM, 2017).

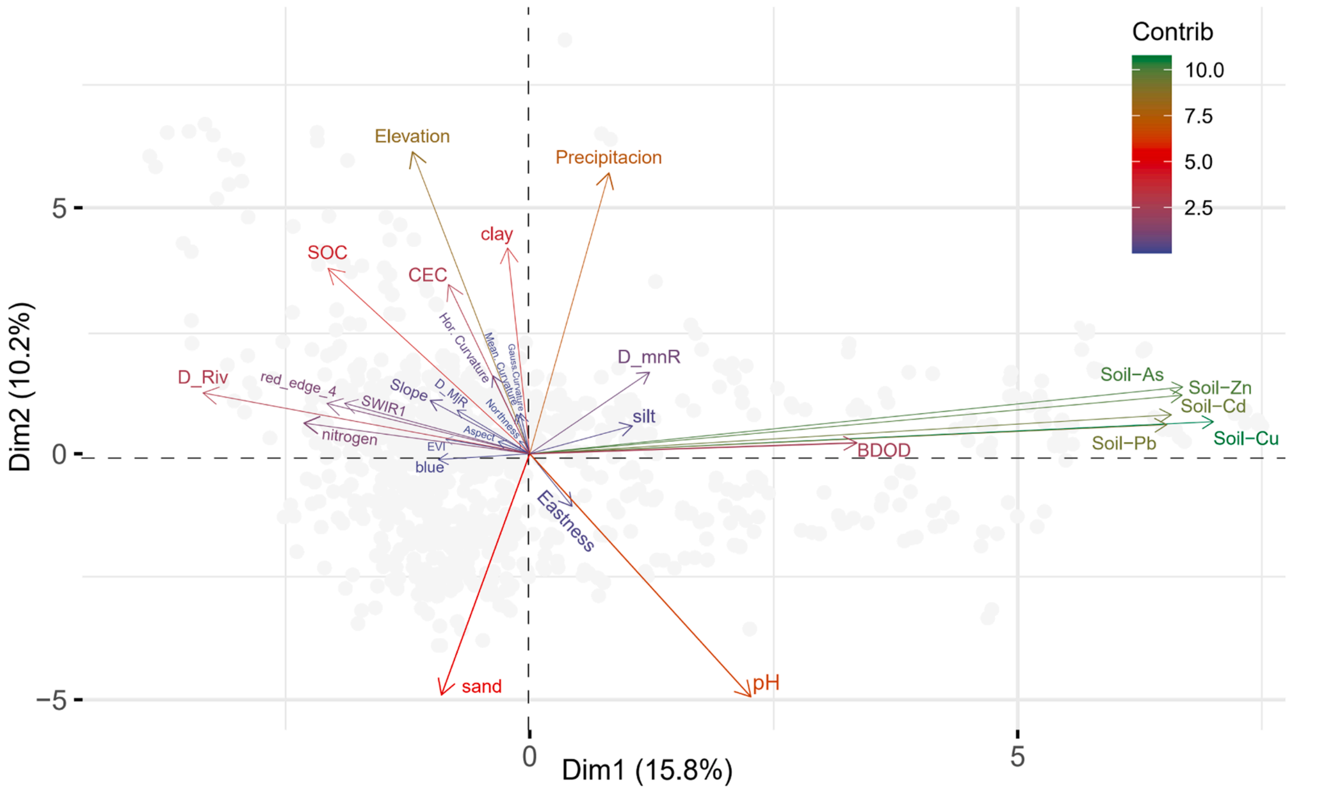

Fig. 2. Relationships among As, Cd, Cu, Pb, and Zn concentrations, soil physicochemical properties, and environmental variables revealed by principal component analysis (PCA) in agricultural soils of the Mantaro Valley. Arrows represent the loadings of the variables.

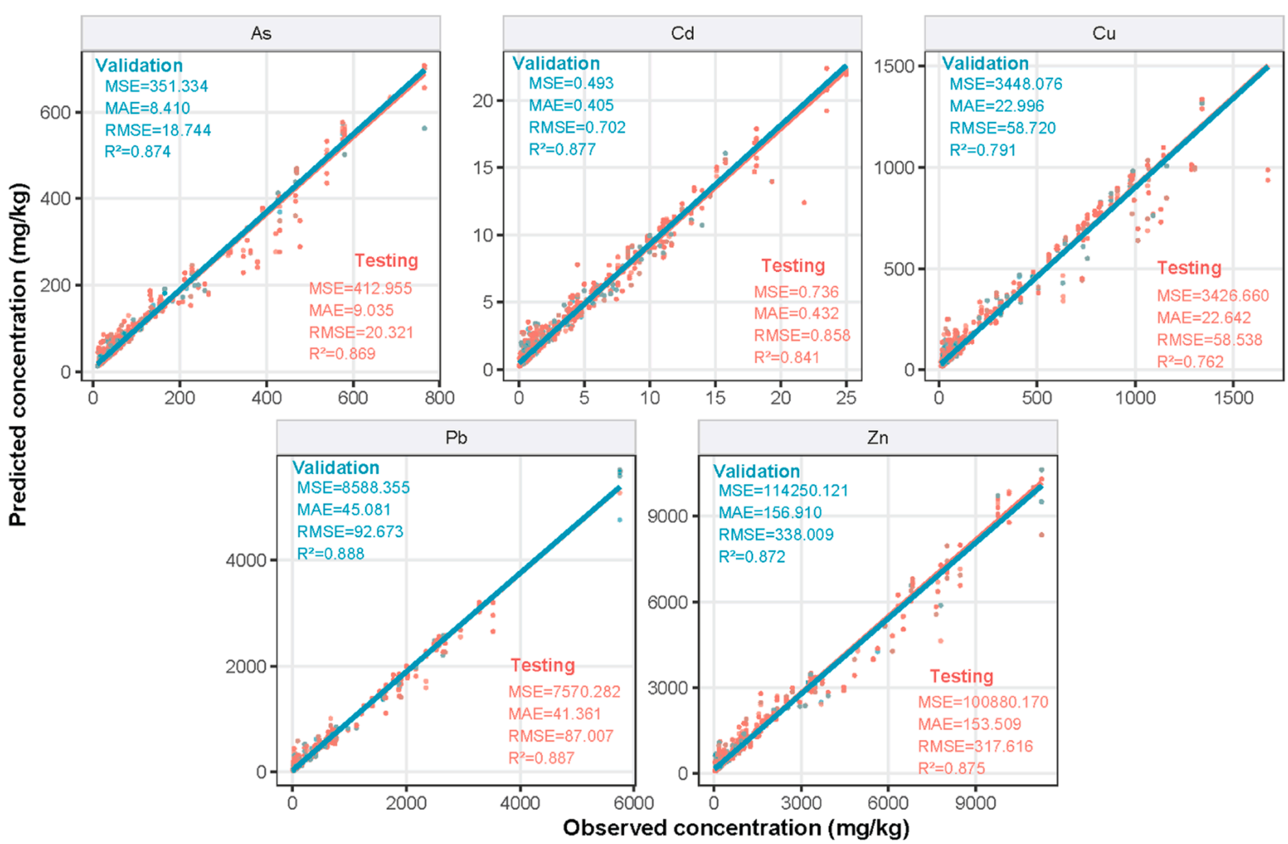

Fig. 3. Performance of Random Forest (RF) models for predicting As, Cd, Cu, Pb, and Zn concentrations in agricultural soils of the Mantaro Valley. Model performance was evaluated using the coefficient of determination (R^2), mean squared error (MSE), mean absolute error (MAE), and root mean squared error (RMSE).

preliminary exploratory patterns consistent with known geochemical behavior, rather than as conclusive evidence of the dominant controls on HM distribution in the Mantaro Valley.

3.3. Performance of RF model for mapping toxic elements

The performance of the RF model for predicting the spatial distribution of As, Cd, Cu, Pb, and Zn in the soils of the Mantaro Valley is presented in Fig. 3, with R^2 values ranging from 0.76 to 0.89. Overall, these values indicate variable predictive capacity, with intermediate to relatively high levels of model fit, depending on the element evaluated. Arsenic and cadmium showed better relative model fit, with R^2 values close to 0.87 and lower prediction errors, particularly Cd, which exhibited the lowest RMSE values (0.70–0.86). Copper showed the lowest relative model fit ($R^2 = 0.76$–0.79) and higher errors, probably associated with its greater variability at elevated concentrations. Lead reached the highest R^2 values, close to 0.89; however, its RMSE values were relatively high (87–93), suggesting that samples with elevated concentrations may have increased the absolute prediction errors. Zinc also showed high RMSE values (318–338), despite R^2 values close to 0.87, indicating that the model captured part of its spatial structure but had limitations in predicting extreme concentrations. Therefore, the RF model provided a useful approximation of HM spatial variability in the soils of the Mantaro Valley, although prediction uncertainty was element-specific and higher for metals with wider concentration ranges. Residuals from the RF predictions are presented in Fig. S2. The residual patterns showed values generally centered around zero for As and Cd, whereas Cu, Pb, and especially Zn exhibited greater dispersion at higher predicted concentrations, indicating element-specific prediction uncertainty. In contrast, Cu, Pb, and especially Zn exhibited increasing residual dispersion at higher predicted concentrations, suggesting that the RF models underestimated extreme values for these elements, consistent with the known tendency of ensemble averaging methods to regress toward the mean at the tails of the concentration distribution. These element-specific bias patterns confirm that prediction uncertainty was highest for metals with wider concentration ranges, and spatial outputs for Zn and Pb in particular should be interpreted with greater caution in areas of high predicted concentration.

3.4. Spatial distribution of toxic elements in agricultural soils applying RF model

The spatial distributions of HMs in the agricultural lands of the Mantaro Valley are shown in Fig. 4. The maps display concentrations in defined intervals, using a color scale where blue tones represent lower concentrations, and yellow, orange, and red tones indicate higher

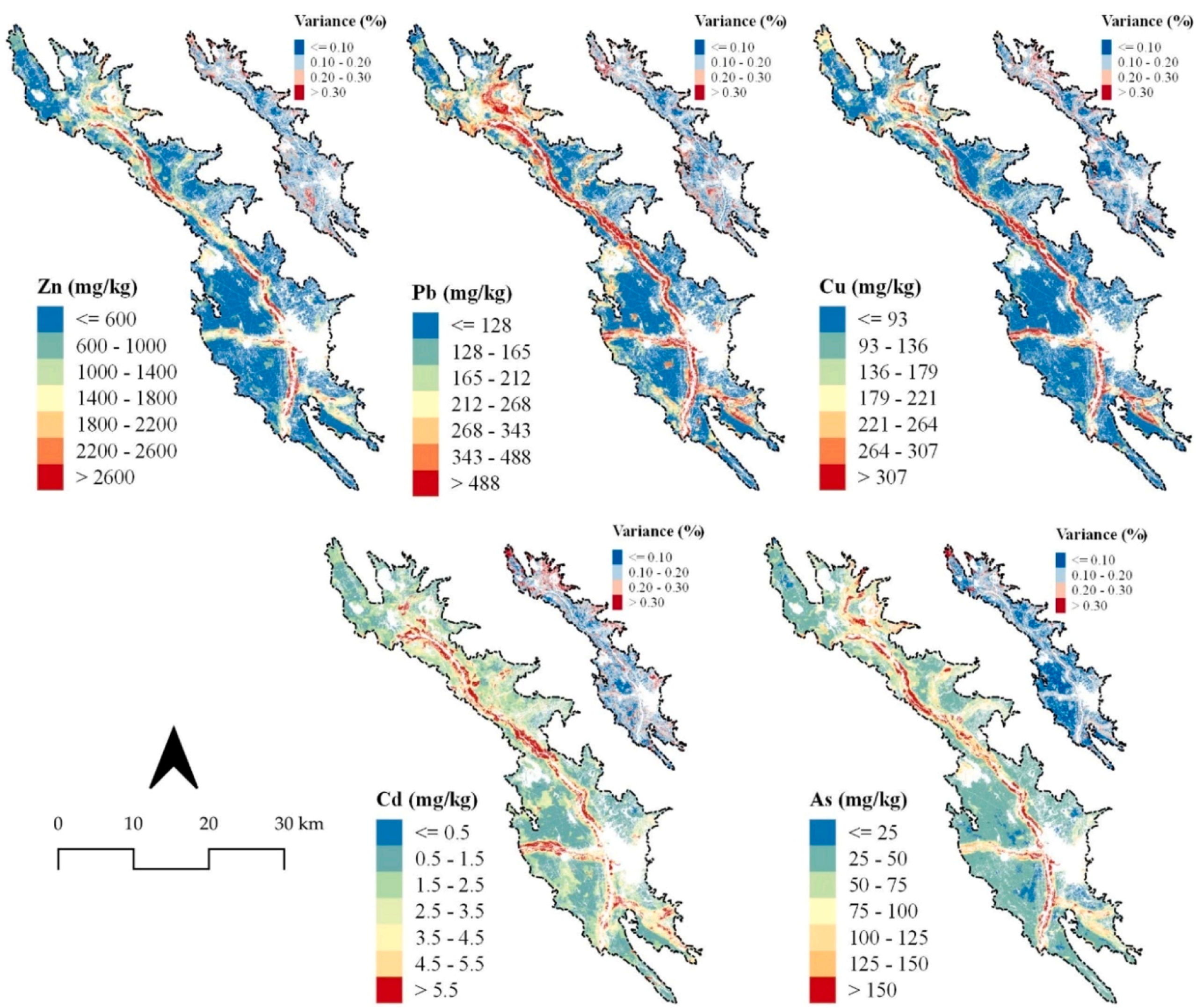

Fig. 4. Spatial distribution of As, Cd, Cu, Pb, and Zn concentrations in agricultural soils predicted using RF models. The inset maps depict the prediction uncertainty of the RF model, expressed as variance (%). Areas with higher variance values indicate greater uncertainty in the predicted concentrations.

concentrations. Zn reached maximum concentrations exceeding 2600 mg kg^{-1}, while the lowest concentrations were below 600 mg kg^{-1}. Similar spatial patterns were observed for Pb and Cu, with maximum values exceeding 488 mg kg^{-1} and 307 mg kg^{-1}, respectively, whereas Cd and As showed more localized areas with concentrations above 5.5 mg kg^{-1} and 150 mg kg^{-1}. These results highlight the spatial heterogeneity of HM accumulation in the valley and suggest the influence of local environmental and land-use factors on contamination patterns.

The uncertainty maps presented in Fig. 4 reflect the spatial variance among k-fold RF predictions and provide a spatially explicit assessment of prediction stability across the study area. Areas with uncertainty values below 5% indicate greater agreement among k-fold predictions and provide stronger support for identifying priority contamination and risk areas. In contrast, zones with uncertainty values above 15% should be interpreted with greater caution, as they reflect higher variability among model predictions. Higher uncertainty was predominantly observed in areas with medium to low predicted concentrations, likely associated with heterogeneous environmental conditions, transitional rural-urban zones, river margins, and agricultural plots with contrasting spectral and soil characteristics. Conversely, zones combining high predicted HM concentrations with low to moderate uncertainty provide the most reliable basis for prioritizing monitoring and risk management interventions.

3.5. Importance variables

Fig. 5 shows the normalized importance of environmental covariates in predicting the spatial distribution of HMs in agricultural soils, according to the selected RF model for each element. The most influential predictors were associated with edaphic properties, hydrological connectivity, and distance-related variables, indicating that HM distribution in the Mantaro Valley is controlled by multiple interacting environmental factors rather than by a single dominant gradient. Edaphic variables such as SOC, pH, nitrogen content, CEC, and soil texture contributed to the prediction of several elements, suggesting that metal retention and accumulation are partly regulated by the soil matrix. This result is consistent with the spatial patterns observed in previous sections, where areas of higher accumulation did not occur uniformly across the valley but were concentrated in specific sectors.

Distance to rivers was one of the most important covariates, particularly for As and Pb, indicating that the Mantaro River and its associated riparian areas may influence the redistribution of contaminants through irrigation, runoff, sediment transport, or historical deposition processes. However, this relationship should be interpreted as an indicator of hydrological connectivity rather than direct evidence of a single contamination source. Road-related covariates also contributed to the prediction of Cd and Cu, suggesting that transport infrastructure, local accessibility, and surrounding land-use intensity may help explain part of the observed spatial variability. Therefore, the variable-importance results support the interpretation that HM accumulation in the Mantaro Valley reflects the combined influence of soil properties, riverine connectivity, agricultural management, and local anthropogenic pressure.

3.6. Spatial distribution of HM contamination levels in agricultural soils

3.6.1. Contamination factor (Cf)

The average contamination factor (Cf) values for the five elements in the agricultural soils of the Mantaro Valley followed the decreasing order As > Cd > Pb > Zn > Cu (Table 3). Except for Cu, the mean Cf values of all analyzed metals exceeded 6, indicating very high contamination levels relative to the selected geochemical background values. In particular, As and Cd showed the highest mean Cf values, suggesting that these elements represent the most relevant contributors to

Table 3
Contamination factor (Cf) classification for each heavy metal in agricultural soils.

HM	Cf			Samples (%)			
	Mean	Min	Max	Cf < 1	1≤ Cf < 3	3≤ Cf <6	Cf ≥6
Zn	14.44	0.37	158.64	5.47	35.37	17.04	42.12
Cd	33.67	0.41	255.10	0.64	5.79	13.50	80.06
Pb	14.80	0.65	287.49	3.86	51.77	16.72	27.65
As	54.23	6.92	509.55	-	-	-	100.00
Cu	6.70	0.43	66.99	13.83	54.66	11.90	19.61

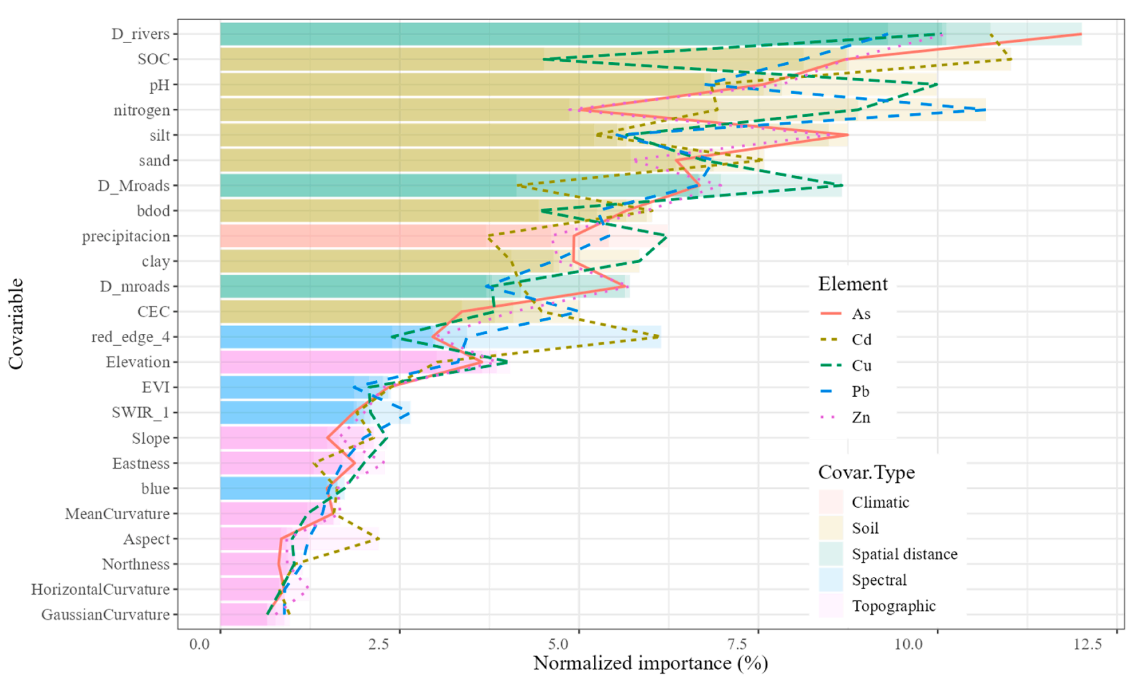

Fig. 5. Normalized importance of environmental covariates in RF models for predicting the spatial distribution of As, Cd, Cu, Pb, and Zn in agricultural soils. Covariates are grouped into climatic, soil, spectral, and topographic categories.

contamination intensity. Significant accumulation, represented by Cf ≥ 6, was observed in 100.00%, 80.06%, 42.12%, 27.65%, and 19.61% of the samples for As, Cd, Zn, Pb, and Cu, respectively. These results indicate that contamination in the valley is not uniform among elements, but is mainly dominated by As and Cd, followed by Zn and Pb (Table S2). The reported contamination levels may be partially influenced by the selection of the geochemical background values used in this study.

The spatial distribution of the contamination factor (Cf) showed heterogeneous patterns across the Mantaro Valley, with significant to very high values predominantly located in the northern sector (Fig. S3). The Cf values for As and Cd showed a relatively continuous distribution, with very high contamination areas extending from north to south along both margins of the Mantaro River. These patterns indicate that contamination was not uniformly distributed among metals, but showed element-specific spatial behavior, and this suggests that the accumulation of these elements in surface soils may reflect the interaction of several environmental and anthropogenic processes, including riverine connectivity, atmospheric deposition, agricultural management, and the redistribution of contaminated particles across the landscape. In this context, previous studies in the Mantaro basin have reported metal enrichment and transport associated with mining-metallurgical activities, river-water contamination, urban emissions, and atmospheric particulate sources, providing relevant background for interpreting the spatial distribution observed in agricultural soils (Álvarez-Tolentino and Suárez-Salas, 2020; Chira et al., 2022; Mallqui Perez et al., 2022; Serrano, 2012).

Significant and very high Cf values for Zn and Pb were mainly observed in the northern, central, and southwestern sectors of the valley, whereas very high Cu contamination was concentrated primarily along the north–south axis in agricultural areas near the Mantaro fluvial system. These patterns indicate that contamination was not uniformly distributed among metals, but showed element-specific spatial behavior. Previous studies have reported that intensive agricultural practices, long-term phosphate fertilizer application, atmospheric deposition, and transport-related activities can contribute to the accumulation of Cd, Pb, Cu, and Zn in agricultural and peri-urban soils (McDowell et al., 2013; McDowell and Gray, 2022; Wang et al., 2020a; Zhou et al., 2024). However, in this study, these references should be interpreted as contextual background, since the identification and quantification of specific sources require additional source-apportionment analyses.

3.6.2. *Geoaccumulation index (Igeo)*

The mean Igeo values followed the order As (4.52) > Cd (3.48) > Zn (1.87) > Pb (1.44) > Cu (0.87) (Table 4). Arsenic exhibited contamination levels ranging from heavily to extremely contaminated, whereas Cd was classified as heavily contaminated. In contrast, Zn and Pb showed moderate contamination levels, while Cu was classified as unpolluted to moderately polluted. Frequency analysis revealed that 24.12% of the samples for As, 21.86% for Cd, and 7.40% for Zn fell within the extremely contaminated category (Igeo ≥ 5). Furthermore, a substantial proportion of As (36.98%) and Cd (14.15%) samples were classified as heavily to extremely contaminated (4 ≤ Igeo < 5). Overall, these results indicate that As and Cd are the primary contributors to geoaccumulation in the agricultural soils of the Mantaro Valley, whereas Pb and Zn exhibit intermediate levels of accumulation, and Cu shows the lowest degree of anthropogenic enrichment. These results are consistent with the Cf patterns and confirm that As and Cd were the most critical elements in terms of contamination relative to the selected geochemical background values. Similar trends have been reported in agricultural soils affected by anthropogenic inputs, including fertilizer application, irrigation-related processes, atmospheric deposition, and traffic-associated emission (He et al., 2024; Hoque et al., 2023; Jing et al., 2023; Mitran et al., 2024).

The spatial distribution of the Igeo showed a pattern generally consistent with the Cf results, with the highest values mainly associated with As and Cd in agricultural areas of the northern and central sectors of the Mantaro Valley (Fig. S4). This agreement indicates that both indices identify similar areas of concern, although Igeo emphasizes the intensity of enrichment relative to the selected background values. In contrast, Zn and Pb showed more localized areas of moderate to high Igeo, whereas Cu exhibited lower and more dispersed Igeo values. Similar patterns have been reported in agricultural soils influenced by repeated fertilizer and pesticide application, irrigation-related processes, traffic-associated emissions, and atmospheric deposition (Taghavi et al., 2023; Vasudhevan et al., 2025; Wang et al., 2020a; Xiao et al., 2019). These findings reinforce that As and Cd were the most critical elements in terms of enrichment, while Pb, Zn, and Cu presented more spatially restricted patterns. The widespread occurrence of As and Cd, together with the greater spatial heterogeneity observed for Pb and Zn, suggests that the processes governing HM transport, retention, and redistribution vary among elements and are likely influenced by their distinct geochemical behavior and local environmental conditions.

3.7. *Spatial distribution of ecological risk (ER) and total ecological risk (RI)*

The ecological risk (ER) assessment for each metal, based on HM concentrations in the agricultural soils of the Mantaro Valley, is presented in Table 5. The results show that 70.10% of Cd samples and 61.41% of As samples were classified as very high ecological risk (ER ≥ 240). In the case of Pb, 57.56% of the samples exhibited low risk, while 15.76%, 7.40%, and 4.50% were classified as moderate, considerable, and high risk, respectively, with an average ER value of 148.01 (Table S3). In contrast, the ecological risks associated with Cu and Zn were predominantly low, with more than 82.00% of the samples falling below critical thresholds. Overall, the ER values ranked the metals in terms of ecological threat as follows: Cd > As > Pb > Cu > Zn, confirming that Cd was the main contributor to ecological risk in the study area, followed by As and Pb. This pattern indicates that ecological risk was not determined solely by the metals with the highest absolute concentrations, but also by their contamination levels and toxic-response coefficients, which explains the dominant contribution of Cd and As. These findings are consistent with those reported by Sanad et al. (2025) in agricultural soils of the Gharb plain in Morocco. Thus, Cd and As represent the most critical elements for ecological monitoring in the agricultural soils of the Mantaro Valley, although their specific sources require further source-oriented analysis.

Regarding the total ecological risk index (RI), sample-level statistics indicate that 71.7% of samples presented RI values exceeding 480,

Table 4
Geoaccumulation index (Igeo) classification for each heavy metal in agricultural soils.

HM	IGEO			Samples (%)						
	Mean	Min	Max	*Igeo*≤ 0	0≤ *Igeo*<1	1≤ *Igeo*<2	2≤ *Igeo*<3	3≤ *Igeo*<4	4≤ *Igeo*<5	*Igeo*≥5
Zn	1.87	- 2.02	6.72	0.96	25.72	16.40	14.15	28.94	6.43	7.40
Cd	3.48	−1.88	7.41	0.96	5.47	12.54	27.01	18.01	14.15	21.86
Pb	1.44	−1.21	7.58	22.51	33.12	15.76	7.40	6.43	5.79	9.00
As	4.52	2.21	8.41	-	-	-	4.82	34.08	36.98	24.12
Cu	0.87	−1.81	5.48	37.62	30.23	11.90	4.18	5.79	9.32	0.96

Table 5
Potential ecological risk (ER) classification for each heavy metal in agricultural soils.

HM	ER			Samples (%)				
	Mean	Min	Max	*ER* < 30	30≤ *ER*<60	60≤ *ER*<120	120≤ *ER*<240	*ER*≥240
Zn	14.4	0.37	158.6	89.39	5.14	5.47	-	-
Cd	1010.2	12.24	7653.0	1.61	1.61	8.68	18.01	70.10
Pb	148.01	6.51	2874.8	57.56	15.76	7.40	4.50	14.79
As	542.30	69.20	5095.5	-	-	5.14	33.44	61.41
Cu	33.51	2.13	334.95	81.99	5.14	4.18	7.40	1.29

corresponding to the very high ecological risk category (Table S4). It is important to note that the percentages reported in Tables 3–5 reflect sample-based classifications, while spatial interpretations derived from RF-predicted maps represent area-based estimates; these two metrics are complementary but not directly comparable, and are treated as such throughout the manuscript. Approximately 34.71% of the evaluated agricultural area presents high ecological risk and 18.67% very high risk, mainly in Jauja, Concepción, Chupaca, and Huancayo provinces (Table S5). Spatially, the northern and central agricultural sectors of the Mantaro Valley were identified as the main areas of ecological concern, consistent with their proximity to historical contamination sources associated with the La Oroya metallurgical complex. It is important to note that the RI values may be partially influenced by the selection of the geochemical background values used in the calculations, as these values directly affect the contamination factors from which the ecological risk estimates are derived.

The spatial distribution pattern of ecological risk associated with HM was heterogeneous (Fig. 6). Areas with very high ecological risk for Cd and As were widely distributed throughout the Mantaro Valley, from north to south. High and very high-risk zones were mainly concentrated in the northern and central parts of the valley, in both irrigated and rainfed agricultural soils. This spatial pattern suggests that ecological risk is not restricted to a single agricultural condition, but reflects the combined influence of metal enrichment, toxicity, hydrological connectivity, agricultural management, and local soil conditions. In this context, the intensive use of agricultural inputs may contribute to the spatial variability of ecological risk in cultivated soils (Sharafi and Salehi, 2025). Moderate and considerable risks for Pb were generally located in the northern part of the valley, particularly in the Jauja area, while high and very high risks were observed along both banks of the Mantaro River in the northern and central zones, possibly associated with atmospheric deposition, heavy traffic on main roads and riverine influence. A relatively uniform risk distribution was observed for Zn and Cu, with predominantly low risk levels. However, moderate Cu-related risks were detected along the valley's longitudinal axis from north to south. Previous studies have reported increased levels of Pb, Zn and Cu in agricultural soils near roads with high traffic density (Fulke et al., 2024; Yan et al., 2018; Zhao et al., 2024).

3.8. Spatial distribution of non-carcinogenic (HI) and carcinogenic (TCR) risk

The spatial distribution of non-carcinogenic and carcinogenic health risks, expressed as HI and TCR, respectively, for Pb, Cd, and As in children and adults is shown in Fig. 7. HQ and CR were calculated as element-specific risk metrics for each exposure pathway, while HI and TCR represent the cumulative non-carcinogenic and carcinogenic risks, respectively. HI values above 1 indicate potential chronic non-carcinogenic effects, whereas TCR values are classified as negligible ($<10^{-6}$), acceptable or tolerable (10^{-6}–10^{-4}), and unacceptable ($>10^{-4}$). The non-carcinogenic risk associated with Cd and Pb remained below the acceptable threshold for both children and adults, indicating limited non-carcinogenic concern for these metals. In contrast, As was the main contributor to HI, with higher values observed in children than in adults. Spatially, higher As-related HI values were mainly concentrated in the northern and southern sectors of the valley, particularly in agricultural soils located along both margins of the Mantaro River. These results indicate that non-carcinogenic risk was mainly driven by As rather than by the metals with the highest absolute concentrations, emphasizing the relevance of toxicity and exposure parameters in health-risk interpretation. Similar patterns have been reported in agricultural soils affected by metal contamination (Ahmad et al., 2025; Chen et al., 2023b; Sanad et al., 2025).

Children showed greater vulnerability to non-carcinogenic and carcinogenic risks than adults. This pattern is consistent with their lower body weight, higher relative exposure rates, and behavioral factors such

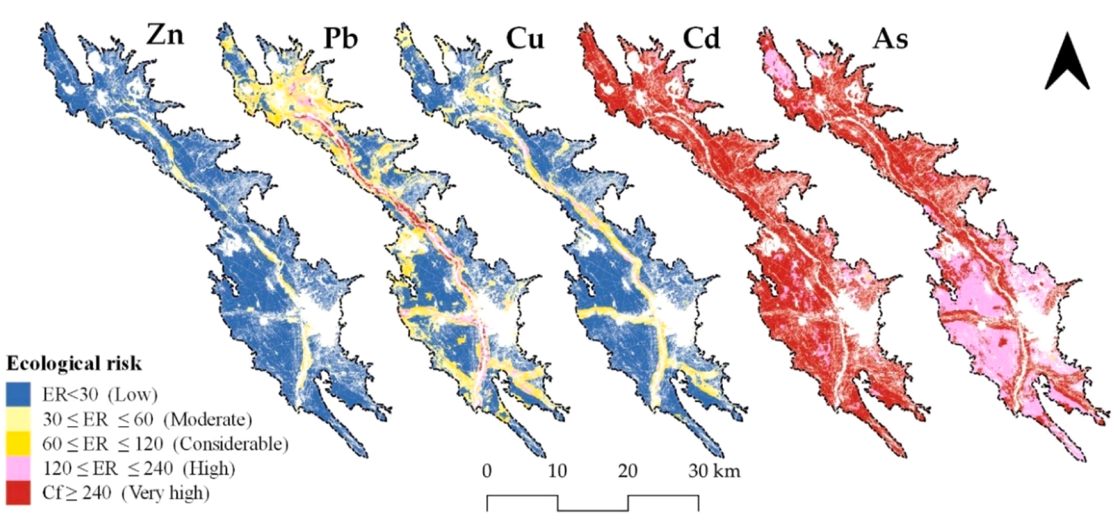

Fig. 6. Spatial distribution of ecological risk (ER) for As, Cd, Cu, Pb, and Zn in agricultural soils of the Mantaro Valley. Higher ER values indicate a greater potential ecological risk associated with each toxic metal.

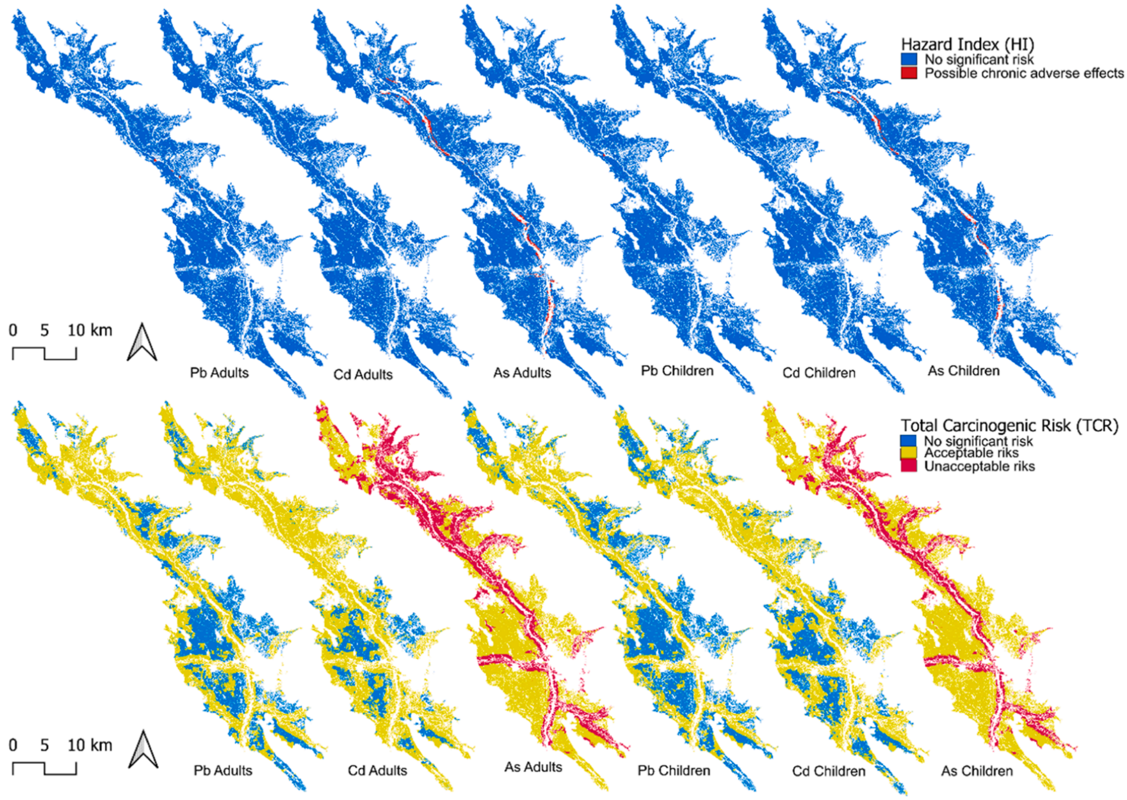

Fig. 7. Spatial distribution of non-carcinogenic (HI) and carcinogenic (TCR) health risks for children and adults associated with exposure to As, Cd, Cu, Pb, and Zn in agricultural soils of the Mantaro Valley. Risk categories were classified according to standard human health risk assessment criteria.

as hand-to-mouth activity, which increase the likelihood of direct soil ingestion (Goyer and Clarkson, 2001; Khatun et al., 2022). In this study, the higher risk values estimated for children indicate that age-specific exposure parameters strongly influence the spatial expression of health risk. Therefore, areas with elevated As-related HI and TCR values should be considered priority zones for health-oriented monitoring, particularly where agricultural activities and residential exposure may overlap (Tepanosyan et al., 2017).

The carcinogenic risk results showed a more critical scenario, with As contributing most strongly to TCR. While Cd and Pb were mainly classified within negligible to acceptable risk levels, As showed areas exceeding the acceptable carcinogenic risk threshold. These higher TCR values were more pronounced in children than in adults and were spatially concentrated mainly in the northern and central sectors of the valley, forming a longitudinal pattern along both margins of the Mantaro River. This pattern is relevant because the Mantaro Valley is intensively cultivated, with up to two cropping seasons per year, which may increase the frequency of soil contact and chronic exposure opportunities among local populations. The dominance of As in TCR is consistent with previous studies reporting carcinogenic risk associated with As-contaminated agricultural soils (Han et al., 2020; More and Dhakate, 2025; Sanad et al., 2025; Sridhar and Parimalarenganayaki, 2024). Given that As is classified as a Group 1 human carcinogen by the International Agency for Research on Cancer, the persistence of areas with unacceptable TCR values highlights the need for targeted soil management, exposure reduction, and monitoring strategies in the Mantaro Valley. The lack of specific exposure parameters for the Peruvian population constitutes a source of uncertainty in health risk estimates, it is recommended that local parameters be developed to improve the accuracy of future assessments.

3.9. Limitations and future perspectives

Although this study provides a spatially explicit assessment of HM contamination and associated ecological and human health risks in agricultural soils of the Mantaro Valley, certain uncertainties and constraints should be considered when interpreting the findings. The sampling design based on Latin Hypercube Sampling represented environmental variability but did not follow a regular grid, so areas with lower sampling density may present greater spatial prediction uncertainty. Soil sampling was limited to the surface layer, which does not allow assessment of vertical metal migration or subsoil accumulation. Future studies could complement these findings through soil profile investigations aimed at evaluating the vertical mobility and leaching behavior of heavy metals and metalloids in Andean agricultural soils. Furthermore, recent advances in multi-sensor data fusion combined with computational classification approaches have shown considerable potential for characterizing subsurface soil conditions and detecting metallic and non-metallic materials at different depths (Khan et al., 2024). The integration of these emerging technologies may improve the understanding of contaminant transport processes beyond the surface layer.

Contamination and ecological risk indices were calculated using Taylor and McLennan (1995) continental crust averages as geochemical background, in the absence of established local baselines for the Mantaro Valley. In mineralized Andean environments, where natural geogenic enrichment of As, Pb, and Zn is well documented, global crustal averages may underestimate natural background concentrations, thereby inflating contamination and enrichment indices. Accordingly, the elevated enrichment factors reported here (43–60 ×) should be interpreted as upper-bound estimates that partly reflect background selection rather than exclusively anthropogenic enrichment (Santos-Francés et al., 2017). Future studies should establish local geochemical baselines from unimpacted Andean reference soils and incorporate probabilistic uncertainty analyses, such as Monte Carlo simulation, to evaluate the robustness of risk classifications (Zhang et al., 2025).

From a spatial modeling perspective, independent field validation would strengthen the spatial reliability of the predicted maps, as model performance may vary across concentration ranges and sampling densities (Han and Suh, 2024). The model performance was evaluated using conventional k-fold cross-validation, and no independent field dataset was available for external validation of the predicted maps. Consequently, the reported accuracy metrics may be influenced by spatial autocorrelation and should be interpreted with appropriate caution. Prediction uncertainty, quantified here as the variance among k-fold RF predictions, was spatially heterogeneous and notably higher in areas with medium to low predicted concentrations, transitional land-use zones, and river margins, reflecting the influence of environmental heterogeneity and sampling density on model stability. Therefore, spatial outputs in these zones should be interpreted with particular caution. Furthermore, uncertainty associated with RF predictions was not formally propagated into the ecological and human health risk assessments, which were conducted using deterministic concentration estimates. Future studies should incorporate independent validation datasets, spatially explicit validation strategies, and uncertainty propagation approaches, such as Monte Carlo simulations, to improve the robustness of spatial risk assessments.

This study relied on a single modeling algorithm. Future studies should evaluate alternative approaches such as XGBoost, support vector machines, or hybrid geostatistical-machine learning methods to further assess model robustness and predictive transferability. Consequently, the relative performance of RF compared with other algorithms remains uncertain. Furthermore, although spatial outputs were generated at 10 m resolution to match the native resolution of the environmental covariates, the effective prediction resolution is inherently constrained by the inter-site sampling spacing of 1–3 km; therefore, the produced maps should be interpreted as screening-level products for identifying priority contamination and risk areas rather than as site-specific predictions at fine spatial scales. The study was based on total metal concentrations and did not assess chemical speciation, bioavailability, or metal mobility, which are critical determinants of environmental risk (Wang et al., 2021). Source attribution is further complicated by naturally mineralized parent material in the central Andes, requiring complementary approaches such as isotopic tracers, mineralogical characterization, sequential extraction, and source-apportionment models such as PMF and UNMIX to distinguish geogenic from anthropogenic contributions (Chen et al., 2022).

The health risk assessment relied on USEPA exposure parameters due to the lack of region-specific exposure factors for the Peruvian population. Although these parameters are widely used and facilitate comparisons with previous studies, they may not fully reflect local demographic characteristics, behavioral patterns, soil ingestion rates, body weight, or exposure frequencies. Consequently, the estimated health risks should be interpreted as screening-level assessments and may differ from actual risks experienced by local populations. Future research should develop and incorporate exposure parameters specific to Peruvian populations, particularly for agricultural communities located in mining-influenced regions. The integration of locally derived exposure factors and probabilistic risk assessment approaches would improve the accuracy and representativeness of human health risk estimates and reduce uncertainty in exposure assessments.

Beyond source characterization, translating contamination assessments into actionable management strategies represents a critical next step. Recent advances in soil remediation have highlighted the potential of composting and organic amendment technologies to reduce contaminant bioavailability and restore soil functionality in polluted agricultural systems (Hadibarata et al., 2025). Although primarily evaluated for organic contaminants such as PAHs, the underlying principles of amendment-driven changes in soil organic matter, pH, and microbial activity are conceptually transferable to HM-contaminated soils, where immobilization and bioavailability reduction are key remediation objectives. Future studies in the Mantaro Valley should therefore evaluate targeted remediation strategies, including composting and phytoremediation, using the present study as a spatial and methodological baseline.

4. Conclusions

The results indicate that agricultural soils in the Mantaro Valley are affected by marked HM contamination, with mean concentrations of Zn, Pb, Cu, As, and Cd exceeding regulatory thresholds and geochemical background values. The RF model provided a useful approximation of HM spatial variability, with R^2 values ranging from 0.76 to 0.89, although prediction uncertainty was element-specific and higher for metals with wider concentration ranges; spatial outputs should be interpreted as screening-level products rather than site-specific predictions. Although Zn, Pb, and Cu showed the highest absolute concentrations, the ecological risk assessment identified Cd and As as the most critical elements due to their high contamination factors and toxic-response coefficients, with 70.10% and 61.41% of samples classified as very high ecological risk, respectively. The total ecological risk index indicated a critical scenario, with 71.7% of samples exceeding the very high-risk threshold. Contamination and ecological risk indices should be interpreted considering their sensitivity to the adopted geochemical background, as the use of global crustal averages may have inflated the magnitude of reported values.

Human health risk assessment identified As as the dominant contributor to both non-carcinogenic and carcinogenic risks, with children showing greater vulnerability than adults. The spatial coincidence between high ecological risk and elevated As-related health risk highlights priority agricultural sectors where monitoring, exposure reduction, and risk-oriented management should be strengthened. Health risk estimates based on USEPA exposure parameters should be considered indicative rather than definitive, given the absence of locally adapted exposure data for agricultural communities in the Mantaro Valley. Therefore, this study provides a spatial and methodological baseline for future investigations aimed at refining local geochemical backgrounds, validating risk estimates, characterizing contamination sources through dedicated source-apportionment approaches, and supporting targeted soil management strategies in the Mantaro Valley.

Funding information

This work was supported by Universidad Nacional del Centro del Perú (CONTRACT N° 13-2022-VRI-UNCP) and, INIA Project "Mejoramiento de los servicios de investigación y transferencia tecnológica en el manejo y recuperación de suelos agrícolas degradados y aguas para riego en la pequeña y mediana agricultura en los departamentos de Lima, Áncash, San Martín, Cajamarca, Lambayeque, Junín, Ayacucho, Arequipa, Puno y Ucayali" CUI 2487112.

CRediT authorship contribution statement

Edith Orellana-Mendoza: Writing – review & editing, Writing – original draft, Supervision, Project administration, Methodology, Investigation, Funding acquisition, Formal analysis, Conceptualization. **Roberto Cosme:** Resources, Methodology, Investigation. **Violeta Quispe-Coquil:** Resources, Methodology, Investigation. **Katia Mendoza:** Resources, Methodology, Investigation. **Sheila Valero-Maraví:** Resources, Methodology, Investigation. **Ángeles Rojas-León:** Resources, Methodology, Investigation. **Dennis Ccopi:** Writing – original draft, Visualization, Formal analysis. **Samuel Pizarro:** Writing – review & editing, Writing – original draft, Funding acquisition, Formal analysis, Data curation.

Declaration of competing interest

The authors declare that they have no known competing financial interests or personal relationships that could have appeared to influence the work reported in this paper.

Also, the authors of the manuscript entitled: "Random Forest-based spatial distribution from heavy metals and associated with ecological and health risk assessment in agricultural soils of the Mantaro Valley, Peru", declare that:

The work described has not been published previously.

The article is not under consideration for publication elsewhere.

The article's publication is approved by all authors and tacitly or explicitly by the responsible authorities where the work was carried out.

If accepted, the article will not be published elsewhere in the same form, in English or in any other language, including electronically, without the written consent of the copyright-holder.

Acknowledgments

The authors express their gratitude to Reginaldo Ayllón, Ruly Curo, Jhosmara Mallqui, Nayelli Huaynalaya, Harold Loardo, Juan Bullón and Cirilo Huaman for providing their support in the collection and preparation of soil samples. They also thank the National Institute of Agricultural Innovation - Ayacucho for the soil analysis.

Supplementary materials

Supplementary material associated with this article can be found, in the online version, at doi:10.1016/j.hazadv.2026.101457.

Data availability

Data will be made available on request.

References

Ahmad, Z., Khan, S.M., Ullah, A., Afza, R., Yang, J., 2025. Source apportionment, carcinogenic and non-carcinogenic risks assessment of soil heavy metals in marble waste polluted environment; role of vegetation in risk mitigation. J. Hazard. Mater. Adv. 18, 100689. https://doi.org/10.1016/j.hazadv.2025.100689.

Alloway, B.J., 2013. In: Alloway, B.J. (Ed.), Heavy Metals in Soils, 3rd ed. Springer. https://doi.org/10.1007/978-94-007-4470-7.

Álvarez-Tolentino, D., Suárez-Salas, L., 2020. Apportionment of emission sources of PM10 and PM2.5 at urban sites of Mantaro Valley, Peru. Rev. Int. Contam. Ambient. 36 (4), 875–892. https://doi.org/10.20937/RICA.53473.

Auritro, S.S., Akter, S., Shemul, S., Chakma, E., Sany, S.R., Ahammed, S., Ara, S., Hawladar, M.F., Hossain, M.N., 2026. Heavy metal toxicity and health risk in water body of Habiganj industrial region: an integrated assessment using spatial modeling, Monte Carlo simulation, and PMF. J. Hazard. Mater. Adv. 21, 101061. https://doi.org/10.1016/j.hazadv.2026.101061.

Breiman, L., 2001. Random forests. Mach. Learn. 45, 5–32. https://doi.org/10.1023/A:1010933404324.

Cai, L.M., Quan, K., Wen, H.H., Luo, J., Wang, S., Chen, L.G., Song, H., Wang, A., 2024. A comprehensive approach for quantifying source-specific ecological and health risks of potentially toxic elements in agricultural soil. Environ. Res. 263, 120163. https://doi.org/10.1016/j.envres.2024.120163.

Carbajal-Llosa, C., Barja, A., Pizarro, S., 2025. Ensemble machine learning for digital mapping of soil pH and electrical conductivity in the Andean agroecosystem of Peru. Front. Soil Sci. 5, 1673628. https://doi.org/10.3389/fsoil.2025.1673628.

Chen, D., Yang, S., Jiang, Z., Wang, Z., Wang, Z., Tian, H., 2023a. Spatial distribution, ecological risk and health risk assessment of heavy metals in agricultural soil from Ankang basin, Shaanxi Province. Heliyon 9, e22580. https://doi.org/10.1016/j.heliyon.2023.e22580.

Chen, D., Wang, X., Luo, X., Huang, G., Tian, Z., Li, W., Liu, F., 2023b. Delineating and identifying risk zones of soil heavy metal pollution in an industrialized region using machine learning. Environ. Pollut. 318, 120932. https://doi.org/10.1016/j.envpol.2022.120932.

Chen, Z., Ding, Y., Jiang, X., Duan, H., Ruan, X., Li, Z., Li, Y., 2022. Combination of UNMIX, PMF model and Pb-Zn-Cu isotopic compositions for quantitative source apportionment of heavy metals in suburban agricultural soils. Ecotoxicol. Environ. Saf. 234, 113369. https://doi.org/10.1016/j.ecoenv.2022.113369.

Chira, J., Vargas, L., Calderón, C., Arcos, F., Mogrovejo, M., De La Cruz, C., 2022. Heavy metals and their impact on surface waters of the Mantaro river basin, Junin, Peru. Int. J. Hydrol. 6 (2), 88–93. https://doi.org/10.15406/ijh.2022.06.00306.

Custodio, M., Huaraca, F., Espinoza, C., Cuadrado, W., 2019. Distribution and accumulation of heavy metals in surface sediment of lake Junín National Reserve, Peru. Open J. Mar. Sci. 09, 33–48. https://doi.org/10.4236/ojms.2019.91003.

Custodio, M., Peñaloza, R., Ochoa, S., Cuadrado, W., 2021. Human risk associated with the ingestion of artichokes grown in soils irrigated with water contaminated by potentially toxic elements, Junin, Peru. Saudi J. Biol. Sci. 28 (10), 5952–5962. https://doi.org/10.1016/j.sjbs.2021.06.054.

Custodio, M., Peñaloza, R., Orellana, E., Aguilar-Cáceres, M.A., Maldonado-Oré, E.M., 2020. Heavy metals and arsenic in soil and cereal grains and potential human risk in the Central region of Peru. J. Ecol. Eng. 22, 206–220. https://doi.org/10.12911/22998993/129255.

Díaz, W., 2016. Estrategia de gestión integrada de suelos contaminados en el Perú. Rev. Del Inst. Investig. FIGMMG-UNMSM 19 (38), 103–110. https://app.ingemmet.gob.pe/biblioteca/pdf/RFIGMMG-38-103.pdf.

Fulke, A.B., Ratanpal, S., Sonker, S., 2024. Understanding heavy metal toxicity: implications on human health, marine ecosystems and bioremediation strategies. Mar. Pollut. Bull. 206, 116707. https://doi.org/10.1016/j.marpolbul.2024.116707.

Gan, L., Wang, J., Xie, M., Yang, B., 2022. Ecological risk and health risk analysis of soil potentially toxic elements from oil production plants in central China. Sci. Rep. 12, 17077. https://doi.org/10.1038/s41598-022-21629-y.

Gao, J., Zhang, D., Proshad, R., Uwiringiyimana, E., Wang, Z., 2021. Assessment of the pollution levels of potential toxic elements in urban vegetable gardens in southwest China. Sci. Rep. 11, 22824. https://doi.org/10.1038/s41598-021-02069-6.

Gong, C., Wang, S., Wang, D., Lu, H., Dong, H., Liu, J., Yan, B., Wang, L., 2022. Ecological and human health risk assessment of heavy metal(loid)s in agricultural soil in hotbed chives hometown of Tangchang, Southwest China. Sci. Rep. 12, 8563. https://doi.org/10.1038/s41598-022-11397-0.

González-Alcaraz, M.N., Loureiro, S., van Gestel, C.A.M., 2018. Toxicokinetics of Zn and Cd in the earthworm Eisenia andrei exposed to metal-contaminated soils under different combinations of air temperature and soil moisture content. Chemosphere 197, 26–32. https://doi.org/10.1016/j.chemosphere.2018.01.019.

Goyer, R.A., Clarkson, T.W., 2001. Toxic effects of metals. Biol. Divers. 2, 811–867. https://doi.org/10.1136/bmj.2.4676.425.

Grimm, R., Behrens, T., Märker, M., Elsenbeer, H., 2008. Soil organic carbon concentrations and stocks on Barro Colorado Island–digital soil mapping using Random Forests analysis. Geoderma 146, 102–113. https://doi.org/10.1016/j.geoderma.2008.05.008.

Hadibarata, T., Syafrudin, M., Fitriyani, N.L., Lee, S.W., 2025. Advancements in composting technologies for efficient soil remediation of polycyclic aromatic hydrocarbons (PAHs): a mini review. Sustainability 17, 5881. https://doi.org/10.3390/su17135881.

Hakanson, L., 1980. An ecological risk index for aquatic pollution control. A sedimentological approach. Water Res. 14 (8), 975–1001. https://doi.org/10.1016/0043-1354(80)90143-8.

Han, H., Suh, J., 2024. Spatial prediction of soil contaminants using a Hybrid random. Appl. Sci. 14, 1666. https://doi.org/10.3390/app14041666.

Han, Q., Wang, M., Cao, J., Gui, C., Liu, Y., He, X., He, Y., Liu, Y., 2020. Health risk assessment and bioaccessibilities of heavy metals for children in soil and dust from urban parks and schools of Jiaozuo, China. Ecotoxicol. Environ. Saf. 191, 110157. https://doi.org/10.1016/j.ecoenv.2019.110157.

He, Y., Wang, W., Chen, Y., Hua, J., Deng, C., Li, H., 2024. Source-sink response analysis of heavy metals and soil pollution assessment in non-ferrous metal industrial agglomeration areas based on decision unit. Sci. Total Environ. 906, 167437. https://doi.org/10.1016/j.scitotenv.2023.167437.

Hengl, T., Nussbaum, M., Wright, M.N., Heuvelink, G.B.M., Gräler, B., 2018. Random forest as a generic framework for predictive modeling of spatial and spatio-temporal variables. PeerJ. 6, e5518. https://doi.org/10.7717/peerj.5518.

Hoque, M.M., Islam, A., Islam, A.R.M.T., Pal, S.C., Mahammad, S., Alam, E., 2023. Assessment of soil heavy metal pollution and associated ecological risk of agriculture dominated mid-channel bars in a subtropical river basin. Sci. Rep. 13, 11104. https://doi.org/10.1038/s41598-023-38058-0.

Huang, Y., Wang, L., Wang, W., Li, T., He, Z., Yang, X., 2019. Current status of agricultural soil pollution by heavy metals in China: a meta-analysis. Sci. Total Environ. 651, 3034–3042. https://doi.org/10.1016/j.scitotenv.2018.10.185.

Huang, Y., He, C., Shen, C., Guo, J., Mubeen, S., Yuan, J., Yang, Z., 2017. Toxicity of cadmium and its health risks from leafy vegetable consumption. Food Funct. 8 (4), 1373–1401. https://doi.org/10.1039/c6fo01580h.

Ishwaran, H., Kogalur, U.B., 2010. Consistency of random rurvival forests. Stat. Probab. Lett. 80, 1056–1064. https://doi.org/10.1016/j.spl.2010.02.020.

Järup, L., 2003. Hazards of heavy metal contamination. Br. Med. Bull. 68, 167–182. https://doi.org/10.1093/bmb/ldg032.

Jiang, H.H., Cai, L.M., Wen, H.H., Luo, J., 2020. Characterizing pollution and source identification of heavy metals in soils using geochemical baseline and PMF approach. Sci. Rep. 10 (1), 6460. https://doi.org/10.1038/s41598-020-63604-5.

Jing, Z., Yi, L.K., Lin, G.C., Jian-Min, Z., Bing, X., 2023. Assessment of potential ecological risk based on the vertical characteristics of potential toxic elements in sediments from a high-density cage culture reservoir in China. Ecotoxicol. Environ. Saf. 262, 115136. https://doi.org/10.1016/j.ecoenv.2023.115136.

Kang, Z., Wang, S., Qin, J., Wu, R., Li, H., 2020. Pollution characteristics and ecological risk assessment of heavy metals in paddy fields of Fujian province, China. Sci. Rep. 10, 12244. https://doi.org/10.1038/s41598-020-69165-x.

Keshavarzi, A., Kumar, V., Ertunç, G., Brevik, E.C., 2021. Ecological risk assessment and source apportionment of heavy metals contamination: an appraisal based on the Tellus soil survey. Environ. Geochem. Health 43, 2121–2142. https://doi.org/10.1007/s10653-020-00787-w.

Khan, M.U., Kamran, M.A., Khan, W.R., Ibrahim, M.M., Ali, M.U., Lee, S.W., 2024. Multi-sensor fusion for remote sensing of metallic and non-metallic object classification in complex soil environments and at different depths. IEEE Trans. Geosci. Remote Sens. 62, 1–13. https://doi.org/10.1109/TGRS.2024.3410530.

Khatun, J., Intekhab, A., Dhak, D., 2022. Effect of uncontrolled fertilization and heavy metal toxicity associated with arsenic(As), lead(Pb) and cadmium (Cd), and possible remediation. Toxicology 477, 153274. https://doi.org/10.1016/j.tox.2022.153274.

Kim, S., Eom, S., Kim, H.J., Lee, J.J., Choi, G., Choi, S., Kim, S., Kim, S.Y., Cho, G., Kim, Y.D., Suh, E., Kim, S.K., Kim, S., Kim, G.H., Moon, H.B., Park, J., Kim, S., Choi, K., Eun, S.H., 2018. Association between maternal exposure to major phthalates, heavy metals, and persistent organic pollutants, and the neurodevelopmental performances of their children at 1 to 2 years of age- CHECK cohort study. Sci. Total Environ. 624, 377–384. https://doi.org/10.1016/j.scitotenv.2017.12.058.

Lemenkova, P., 2024. Support vector machine algorithm for mapping land cover dynamics in Senegal, west Africa, using earth observation data. Earth 5 (3), 420–462. https://doi.org/10.3390/earth5030024.

Li, D., Lu, Q., Cai, L., Chen, L., Wang, H., 2023. Characteristics of soil heavy metal pollution and health risk assessment in urban parks at a megacityof Central China. Toxics 11, 257. https://doi.org/10.3390/toxics11030257.

Li, J., Li, X., Wang, C., Liu, J.Z., Gao, Z.D., Li, K.M., Tuo, X.Y., Zang, F., 2024a. Pollution characteristics and probabilistic risk assessment of heavy metal(loid)s in agricultural soils across the Yellow River Basin, China. Ecol. Indic. 167, 112676. https://doi.org/10.1016/j.ecolind.2024.112676.

Li, W., Zhang, S., Gao, F., Chen, Z., Jiang, J., Sun, G.X., 2024b. Spatial distribution, sources apportionment and risk assessment of heavy metals in the Changchun black soil area, China. J. Hazard. Mater. Adv. 13, 100402. https://doi.org/10.1016/j.hazadv.2024.100402.

Li, X., Gu, H., Tang, R., Zou, B., Liu, X., Ou, H., Chen, X., Song, Y., Luo, W., Wen, B., 2025a. A fusion XGBoost approach for large-scale monitoring of soil heavy metal in farmland using hyperspectral imagery. Agronomy 15, 676. https://doi.org/10.3390/agronomy15030676.

Li, Y., Yu, Y., Ding, S., Dai, W., Shi, R., Cui, G., Li, X., 2025b. Application of machine learning in soil heavy metals pollution assessment in the southeastern Tibetan plateau. Sci. Rep. 15, 13579. https://doi.org/10.1038/s41598-025-97006-2.

Liu, J., Kang, H., Tao, W., Li, H., He, D., Ma, L., Tang, H., Wu, S., Yang, K., Li, X., 2023. A spatial distribution–Principal component analysis (SD-PCA) model to assess pollution of heavy metals in soil. Sci. Total Environ. 859, 160112. https://doi.org/10.1016/j.scitotenv.2022.160112.

Liu, S., Bliss, N., Sundquist, E., Huntington, T.G., 2003. Modeling carbon dynamics in vegetation and soil under the impact of soil erosion and deposition. Glob. Biogeochem. Cycles 17 (2), 1–24. https://doi.org/10.1029/2002gb002010.

Liu, T., Wang, Z., 2024. Contamination and health risk assessment of heavy metals in soil surrounding an electroplating factory in JiaXing, China. Sci. Rep. 14, 4097. https://doi.org/10.1038/s41598-024-54620-w.

Loayza Muro, R., 2016. Daños ambientales de la minería en el Perú: ¿qué hacer con ellos? In Consorcio de Universidades. Metas Del Perú al Bicentenario. Consorcio de Universidades, p. 336. http://www.consorcio.edu.pe/metas-bicentenario/Metas-del-Peru-al-Bicentenario-Consorcio-de-Universidades-Libro-Digital.pdf.

Louppe, G. (2014). Understanding random forests: from theory to practice [University of Liège]. http://arxiv.org/abs/1407.7502.

Mallqui Perez, J.F., Miguel Lizana, Y., & Reyes Leydi, S.L. (2022). Análisis espacio temporal de la calidad de agua del río Mantaro influenciada por las aguas residuales del año 2004 - 2008 y 2015 - 2019 [Universidad Continental]. https://repositorio.continental.edu.pe/bitstream/20.500.12394/11987/2/IV_FIN_107_TE_Mallqui_Miguel_Reyes_2022.pdf.

McDowell, R.W., Gray, C.W., 2022. Do soil cadmium concentrations decline after phosphate fertiliser application is stopped: a comparison of long-term pasture trials in New Zealand? Sci. Total Environ. 804, 150047. https://doi.org/10.1016/j.scitotenv.2021.150047.

McDowell, R.W., Taylor, M.D., Stevenson, B.A., 2013. Natural background and anthropogenic contributions of cadmium to New Zealand soils. Agric. Ecosyst. Environ. 165, 80–87. https://doi.org/10.1016/j.agee.2012.12.011.

MINAGRI. (2011). Estudio de conformación de bloques de riego para la formalización de derechos de uso de agua en el valle alto Santa sector de riego Huaraz.

MINAM, 2014. Soil Sampling Guide. Ministry of the Environment. http://www.minam.gob.pe/wp-content/uploads/2014/04/GUIA-MUESTREO-SUELO_MINAM1.pdf.

MINAM, 2017. Environmental quality standards for soil in Peru. El Peruano. http://www.minam.gob.pe/wp-content/uploads/2017/12/DS_011-2017-MINAM.pdf.

Mitran, T., Gunnam, J.R.S., Gourigari, S., Kandrika, S., 2024. Assessment of depth wise distribution, enrichment, contamination, ecological risk and sources of soil heavy metals over an industrial area in Southern India. J. Geochem. Explor. 257, 107379. https://doi.org/10.1016/j.gexplo.2023.107379.

More, S., Dhakate, R., 2025. Geogenic and anthropogenic sources of heavy metals in soil: an ecological and health risk assessment in the granitic terrain of South India. Catena 254, 108960. https://doi.org/10.1016/j.catena.2025.108960.

Muller, G., 1969. Index of geoaccumulation in sediments of the Rhine River. GeoJournal 2, 108–118. https://www.scienceopen.com/document?vid=4b875795-5729-4c05-9813-64951e2ca488.

Mushak, P., 2011. Lead toxicity in humans: a brief historical perspective and public health context. In: Trace Metals and Other Contaminants in the Environment, 10. Elsevier, pp. 401–437. https://doi.org/10.1016/B978-0-444-51554-4.00011-0.

Nagajyoti, P.C., Lee, K.D., Sreekanth, T.V.M., 2010. Heavy metals, occurrence and toxicity for plants: a review. Environ. Chem. Lett. 8, 199–216. https://doi.org/10.1007/s10311-010-0297-8.

Nematollahi, M.J., Keshavarzi, B., Zaremoaiedi, F., Rajabzadeh, M.A., Moore, F., 2020. Ecological-health risk assessment and bioavailability of potentially toxic elements (PTEs) in soil and plant around a copper smelter. Environ. Monit. Assess. 192, 639. https://doi.org/10.1007/s10661-020-08589-4.

Nguyen, H.T.T., Doan, T.M., Tomppo, E., McRoberts, R.E., 2020. Land use/land cover mapping using multitemporal sentinel-2 imagery and four classification methods-A case study from Dak Nong, Vietnam. Remote Sens. 12 (9), 1367. https://doi.org/10.3390/RS12091367.

Oguntuase, M.A., Oyebamiji, A.O., Ayeni, O.M., Adeyanju, O.T., 2024. A comprehensive environmental analysis of heavy metal contamination, ecological risks and health impacts in Ilokun area, Ado-Ekiti, Nigeria. Environ. Pollut. Manag. 1, 118–127. https://doi.org/10.1016/j.epm.2024.08.004.

Orellana, E., Custodio, M., Bastos, M.C., Cuadrado, W., 2019. Lead in agricultural soils and cultivated pastures irrigated with river water contaminated by mining activity. J. Ecol. Eng. 20 (8), 238–244. https://doi.org/10.12911/22998993/111715.

Pizarro, S., Pricope, N.G., Figueroa, D., Carbajal, C., Quispe, M., Vera, J., Alejandro, L., Achallma, L., Gonzalez, I., Salazar, W., Loayza, H., Cruz, J., Arbizu, C.I., 2023. Implementing cloud computing for the digital mapping of agricultural soil properties from high resolution UAV multispectral imagery. Remote Sens. 15, 3203. https://doi.org/10.3390/rs15123203.

Pizarro, S., Pricope, N.G., Vera, J., Cruz, J., Lastra, S., Solórzano-Acosta, R., Martínez, P. V., 2025a. Comprehensive spatial mapping of metals and metalloids in the Peruvian Mantaro Valley using advanced geospatial data integration. Geoderma 453, 117138. https://doi.org/10.1016/j.geoderma.2024.117138.

Pizarro, S., Requena-Rojas, E., Barboza, E., Peña-Elme, E., Arias-Arredondo, A., Ccopi, D., 2025b. Ecological and carcinogenic risk assessment of potentially toxic elements in rangelands and croplands around Lake Junin (Peru): integrating remote sensing, machine learning, and land cover segmentation. Sci. Total Environ. 999, 180327. https://doi.org/10.1016/j.scitotenv.2025.180327.

Qu, L., Lu, H., Tian, Z., Schoorl, J.M., Huang, B., Liang, Y., Qiu, D., Liang, Y., 2024a. Spatial prediction of soil sand content at various sampling density based on geostatistical and machine learning algorithms in plain areas. Catena 234, 107572. https://doi.org/10.1016/j.catena.2023.107572.

Qu, X., Niu, Q., Sheng, C., Xia, M., Zhang, C., Qu, X., Yang, C., 2024b. Co-toxicity and co-contamination remediation of polycyclic aromatic hydrocarbons and heavy metals: research progress and future perspectives. Environ. Res. 263, 120211. https://doi.org/10.1016/j.envres.2024.120211.

R Core Team, 2023. R: A Language and Environment for Statistical Computing. R Foundation for Statistical Computing. https://www.r-project.org/.

Rammal, J., Diab, W., Nasser, G., Baki, Z.A., El Badan, D., Haidar, C., Hijazi, A., 2025. Transport pathways and bioavailability of soil-borne heavy metals in agricultural systems. J. Appl. Organomet. Chem. 5 (3), 368–391. https://doi.org/10.48309/jaoc.2025.524695.1297.

Reuer, M.K., Bower, N.W., Koball, J.H., Hinostroza, E., De la Torre Marcas, M.E., Surichaqui, J.A.H., Echevarria, S., 2012. Lead, arsenic, and cadmium contamination and its impact on children's health in La Oroya, Peru. ISRN Public Health 2012, 1–12. https://doi.org/10.5402/2012/231458.

Rezapour, S., Siavash Moghaddam, S., Nouri, A., Khosravi Aqdam, K., 2022. Urbanization influences the distribution, enrichment, and ecological health risk of heavy metals in croplands. Sci. Rep. 12, 3868. https://doi.org/10.1038/s41598-022-07789-x.

Ruelas-Inzunza, J., Spanopoulos-Zarco, P., Páez-Osuna, F., 2009. Cd, Cu, Pb and Zn in clams and sediments from an impacted estuary by the oil industry in the southwestern Gulf of Mexico: concentrations and bioaccumulation factors. J. Environ. Sci. Health Part A Toxic/Hazard. Subst. Environ. Eng. 44 (14), 1503–1511. https://doi.org/10.1080/10934520903263280.

Sanad, H., Moussadek, R., Mouhir, L., Lhaj, M.O., Zahidi, K., Dakak, H., Manhou, K., Zouahri, A., 2025. Ecological and human health hazards evaluation of toxic metal contamination in agricultural lands using multi-index and geostatistical techniques across the Mnasra area of Morocco's Gharb plain region. J. Hazard. Mater. Adv. 18, 100724. https://doi.org/10.1016/j.hazadv.2025.100724.

Sandoval, F.M., Mucha, L.F., Platero, I.Y., 2022. Evaluation of the behavior of climatic elements in the Mantaro Valley from 2000 to 2020, department of Junín. IOP Conf. Ser.: Earth Environ. Sci. 1072, 012007. https://doi.org/10.1088/1755-1315/1072/1/012007.

Santos-Francés, F., Martínez-Graña, A., Rojo, P.A., Sánchez, A.G., 2017. Geochemical background and baseline values determination and spatial distribution of heavy metal pollution in soils of the andes mountain range (Cajamarca-Huancavelica, Peru). Int. J. Environ. Res. Public Health 14, 859. https://doi.org/10.3390/ijerph14080859.

Serrano, F. (2012). The impact of environmental contamination on public health and environmental quality in La Oroya and the Mantaro watershed. chrome-extension://efaidnbmnnnibpcajpcglclefindmkaj/ https://aida-americas.org/sites/default/files/featured_pubs/adjunto_4_aida_impacto_de_la_contaminacion_sobre_la_salud_y_el_ambiente_en_la_oroya_y_la_cuenca_del_rio_mantaro._testimonio_del_dr._fernando_se.

Shaikh, J., Yamsani, S.K., Bora, M.J., Sahoo, S., Sekharan, S., Rakesh, R.R., 2021. Influence of infiltration on soil erosion in green infrastructures. Acta Hortic. Regiotect. 24, 1–8. https://doi.org/10.2478/ahr-2021-0018.

Sharafi, S., Salehi, F., 2025. Comprehensive assessment of heavy metal (HMs) contamination and associated health risks in agricultural soils and groundwater proximal to industrial sites. Sci. Rep. 15, 7518. https://doi.org/10.1038/s41598-025-91453-7.

Sharafi, S., Sharafi, M., Lorvand, M., 2026. Soil-water-crop pathways of heavy metal contamination and human health risks in intensive smallholder farms of the Nahavand Plain, Iran. Sci. Rep. 16, 9947. https://doi.org/10.1038/s41598-026-38637-x.

Shi, T., Hu, X., Guo, L., Su, F., Tu, W., Hu, Z., Liu, H., Yang, C., Wang, J., Zhang, J., Wu, G., 2021. Digital mapping of zinc in urban topsoil using multisource geospatial data and random forest. Sci. Total Environ. 792, 148455. https://doi.org/10.1016/j.scitotenv.2021.148455.

Sridhar, D., Parimalarenganayaki, S., 2024. Evaluation of human and ecological health risks associated with the potentially toxic heavy metals in groundwater of Vellore city, Tamil Nadu, India. J. Hazard. Mater. Adv. 16, 100497. https://doi.org/10.1016/j.hazadv.2024.100497.

Taghavi, M., Darvishiyan, M., Momeni, M., Eslami, H., Fallahzadeh, R.A., Zarei, A., 2023. Ecological risk assessment of trace elements (TEs) pollution and human health risk exposure in agricultural soils used for saffron cultivation. Sci. Rep. 13, 4556. https://doi.org/10.1038/s41598-023-31681-x.

Taghizadeh-Mehrjardi, R., Fathizad, H., Hakimzadeh Ardakani, M.A., Sodaiezadeh, H., Kerry, R., Heung, B., Scholten, T., 2021. Spatio-temporal analysis of heavy metals in arid soils at the catchment scale using digital soil assessment and a random forest model. Remote Sens. 13, 1698. https://doi.org/10.3390/rs13091698.

Tang, J., Zhang, J., Ren, L., Zhou, Y., Gao, J., Luo, L., Yang, Y., Peng, Q., Huang, H., Chen, A., 2019. Diagnosis of soil contamination using microbiological indices: a review on heavy metal pollution. J. Environ. Manag. 242, 121–130. https://doi.org/10.1016/j.jenvman.2019.04.061. April.

Taylor, S.R., McLennan, S.M., 1995. The geochemical the continental evolution crust. Rev. Geophys. 33 (2), 241–265. https://doi.org/10.1029/95RG00262.

Tepanosyan, G., Maghakyan, N., Sahakyan, L., Saghatelyan, A., 2017. Heavy metals pollution levels and children health risk assessment of Yerevan kindergartens soils. Ecotoxicol. Environ. Saf. 142, 257–265. https://doi.org/10.1016/j.ecoenv.2017.04.013.

Udeigwe, T.K., Eze, P.N., Teboh, J.M., Stietiya, M.H., 2011. Application, chemistry, and environmental implications of contaminant-immobilization amendments on agricultural soil and water quality. Environ. Int. 37, 258–267. https://doi.org/10.1016/j.envint.2010.08.008.

USEPA, 2001. Risk Assessment Guidance for Superfund: Volume III–Part A, Process for Conducting Probabilistic Risk Assessment. United States Environmental Protection Agency, p. 385. https://semspub.epa.gov/work/HQ/134487.pdf.

USEPA, 2007. Microwave Assisted Acid Digestion of Sediments, Sludges, Soils and Oils. United States Enviromental Protecction Agency. https://www.epa.gov/sites/production/files/2015-12/documents/3051a.pdf.

USEPA, 2019. Guideline for Human Exposure Assessment. Unites States Of Environmental Protection Agency, p. 199. https://www.epa.gov/sites/default/files/2020-01/documents/guidelines_for_human_exposure_assessment_final2019.pdf.

Vasudhevan, P., Pu, S., Ayyamperumal, R., Manikandan, E., Sujitha, S.B., Singh, S., Ponniah, J.M., Dixit, S., Thangavel, P., 2025. Pollution assessment, ecological risk and source identification of heavy metals in paddy soils and rice grains from Salem, South India. J. Hazard. Mater. Adv. 17, 100526. https://doi.org/10.1016/j.hazadv.2024.100526.

Wang, C.X., Liu, F., Cheng, Y., Cao, L., Wu, H., 2025a. Investigation and evaluation of the healthy risk of heavy metal contents in astragalus membranaceus of Shaanxi province. J. Food Prot. 88, 100563. https://doi.org/10.1016/j.jfp.2025.100563.

Wang, F., Guan, Q., Tian, J., Lin, J., Yang, Y., Yang, L., Pan, N., 2020a. Contamination characteristics, source apportionment, and health risk assessment of heavy metals in agricultural soil in the Hexi Corridor. Catena 191, 104573. https://doi.org/10.1016/j.catena.2020.104573.

Wang, H., Yilihamu, Q., Yuan, M., Bai, H., Xu, H., Wu, J., 2020b. Prediction models of soil heavy metal(loid)s concentration for agricultural land in Dongli: a comparison of regression and random forest. Ecol. Indic. 119, 106801. https://doi.org/10.1016/j.ecolind.2020.106801.

Wang, J., Wang, B., Zhao, Q., Cao, J., Xiao, X., Zhao, D., Chen, Z., Wu, D., 2025b. Sources analysis and risk assessment of heavy metals in soil in a polymetallic mining area in southeastern Hubei based on Monte Carlo simulation. Ecotoxicol. Environ. Saf. 290, 117607. https://doi.org/10.1016/j.ecoenv.2024.117607.

Wang, J.X., Xu, D.M., Fu, R.B., Chen, J.P., 2021. Bioavailability assessment of heavy metals using various multi-element extractants in an indigenous zinc smelting contaminated site, southwestern China. Int. J. Environ. Res. Public Health 18, 8560. https://doi.org/10.3390/ijerph18168560.

Wang, S., Wang, L., Liao, X., Zhou, G., Huan, Y., Li, S., Liang, T., 2025c. Impact of residential density on heavy metal mobilization in urban soils: human activity patterns and eco-health risks in the Beijing-Tianjin-Hebei region. Ecotoxicol. Environ. Saf. 302, 118559. https://doi.org/10.1016/j.ecoenv.2025.118559. June.

Wei, W., Ling, S., Wu, X., Li, X., 2023. Geochemical accumulation and source tracing of heavy metals in arable soils from a black shale catchment, southwestern China. Sci. Total Environ. 857, 159467. https://doi.org/10.1016/j.scitotenv.2022.159467.

Wu, Q., Hu, W., Wang, H., Liu, P., Wang, X., Huang, B., 2021. Spatial distribution, ecological risk and sources of heavy metals in soils from a typical economic development area, Southeastern China. Sci. Total Environ. 780, 146557. https://doi.org/10.1016/j.scitotenv.2021.146557.

Xiao, R., Guo, D., Ali, A., Mi, S., Liu, T., Ren, C., Li, R., Zhang, Z., 2019. Accumulation, ecological-health risks assessment, and source apportionment of heavy metals in paddy soils: a case study in Hanzhong, Shaanxi, China. Environ. Pollut. 248, 349–357. https://doi.org/10.1016/j.envpol.2019.02.045.

Xu, X., Wang, Z., Song, X., Zhan, W., Yang, S., 2024. A remote sensing-based strategy for mapping potentially toxic elements of soils: temporal-spatial-spectral covariates combined with random forest. Environ. Res. 240, 117570. https://doi.org/10.1016/j.envres.2023.117570.

Yan, G., Mao, L., Liu, S., Mao, Y., Ye, H., Huang, T., Li, F., Chen, L., 2018. Enrichment and sources of trace metals in roadside soils in Shanghai, China: a case study of two urban/rural roads. Sci. Total Environ. 631–632, 942–950. https://doi.org/10.1016/j.scitotenv.2018.02.340.

Yang, S., Taylor, D., Yang, D., He, M., Liu, X., Xu, J., 2021. A synthesis framework using machine learning and spatial bivariate analysis to identify drivers and hotspots of heavy metal pollution of agricultural soils. Environ. Pollut. 287, 117611. https://doi.org/10.1016/j.envpol.2021.117611. June.

Ye, M., Zhu, L., Li, X., Ke, Y., Huang, Y., Chen, B., Yu, H., Li, H., Feng, H., 2023. Estimation of the soil arsenic concentration using a geographically weighted XGBoost model based on hyperspectral data. Sci. Total Environ. 858, 159798. https://doi.org/10.1016/j.scitotenv.2022.159798.

Yu, T.K., Chang, I.C., De Chen, S., Chen, H.L., Yu, T.Y., 2025. Predicting potential soil and groundwater contamination risks from gas stations using three machine learning models (XGBoost, LightGBM, and Random Forest). Process Saf. Environ. Prot. 199, 107249. https://doi.org/10.1016/j.psep.2025.107249.

Zerizghi, T., Guo, Q., Tian, L., Wei, R., Zhao, C., 2022. An integrated approach to quantify ecological and human health risks of soil heavy metal contamination around coal mining area. Sci. Total Environ. 814, 152653. https://doi.org/10.1016/j.scitotenv.2021.152653.

Zhang, H., Mao, Z., Huang, K., Wang, X., Cheng, L., Zeng, L., Zhou, Y., Jing, T., 2019. Multiple exposure pathways and health risk assessment of heavy metal(loid)s for children living in fourth-tier cities in Hubei Province. Environ. Int. 129, 517–524. https://doi.org/10.1016/j.envint.2019.04.031.

Zhang, H., Yin, S., Chen, Y., Shao, S., Wu, J., Fan, M., Chen, F., Gao, C., 2020. Machine learning-based source identification and spatial prediction of heavy metals in soil in a rapid urbanization area, eastern China. J. Clean. Prod. 273, 122858. https://doi.org/10.1016/j.jclepro.2020.122858.

Zhang, T., Wang, P., Wang, M., Liu, J., Gong, L., Xia, S., 2023. Spatial distribution, source identification, and risk assessment of heavy metals in riparian soils of the Tibetan plateau. Environ. Res. 237, 116977. https://doi.org/10.1016/j.envres.2023.116977.

Zhang, W., Xin, C., Du, W., Yu, S., 2025. Health risk assessment of heavy metals based on source analysis and Monte Carlo in the Lijiang River Basin, China. Ecol. Indic. 176, 113620. https://doi.org/10.1016/j.envres.2023.117975.

Zhao, J., Cao, C., Chen, X., Zhang, W., Ma, T., Irfan, M., Zheng, L., 2024. Source-specific ecological risk analysis and critical source identification of heavy metal(loid)s in the soil of typical abandoned coal mining area. Sci. Total Environ. 947, 174506. https://doi.org/10.1016/j.scitotenv.2024.174506.

Zhao, X., Li, Z., Wang, D., Li, J., Zou, B., Tao, Y., Lei, L., Qiao, F., Huang, J., 2019. Assessment of residents' total environmental exposure to heavy metals in China. Sci. Rep. 9, 16386. https://doi.org/10.1038/s41598-019-52649-w.

Zhou, W., Yu, R., Guo, F., Shen, C., Liu, Y., Huang, Y., 2024. Source apportionment and risk assessment of soil heavy metals in the Huangshui River Basin using a hybrid model. Ecol. Indic. 160, 111906. https://doi.org/10.1016/j.ecolind.2024.111906.

Zhuang, H., Wang, Y., Liu, H., Wang, S., Zhang, W., Zhang, S., Dai, Q., 2021. Large-scale soil erosion estimation considering vegetation growth cycle. Land 10, 473. https://doi.org/10.3390/land10050473.